eNeuro

Research Article: New Research | Sensory and Motor Systems

GluA2-containing AMPA receptors distinguish ribbon-associated from ribbon-less afferent contacts on rat cochlear hair cells

Diversity of afferent contacts on outer hair cells

Rodrigo Martinez-Monedero[1,*], Chang Liu[2,*], Catherine Weisz[2], Pankhuri Vyas[2], Paul Albert Fuchs[2] and Elisabeth Glowatzki[2]

[1]*Department of Neuroscience, The Johns Hopkins University School of Medicine, Baltimore, Maryland 21205*
[2]*Department of Otolaryngology, Head and Neck Surgery, The Center for Hearing and Balance and the Center for Sensory Biology, Institute for Basic Biomedical Sciences, Baltimore, Maryland 21205*

DOI: 10.1523/ENEURO.0078-16.2016

Received: 12 April 2016

Accepted: 26 April 2016

Published: 9 May 2016

Author contributions: R.M.-M., C.L., C.W., P.V., and E.G. designed research; R.M.-M., C.L., C.W., and P.V. performed research; R.M.-M., C.L., C.W., P.V., P.A.F., and E.G. analyzed data; R.M.-M., C.L., P.V., P.A.F., and E.G. wrote the paper.

Funding: National Institute for Deafness and Other Communication Disorders: R01DC006476. National Institute for Deafness and Other Communication Disorders: R01DC011741. National Institute for Deafness and Other Communication Disorders: T32DC000023. National Institute for Deafness and Other Communication Disorders: F31DC010948. NINDS: NS050274. the John Mitchell Junior Trust; National Institute for Deafness and Other Communication Disorders: P30DC005211.

Conflict of Interest: The authors declare no conflicting financial interests.

*R.M.-M. and C.L. are co-first authors.

Correspondence should be addressed to either Elisabeth Glowatzki or Paul Albert Fuchs, the Center for Hearing and Balance, Department of Otolaryngology, Head and Neck Surgery, and the Center for Sensory Biology, Institute for Basic Biomedical Sciences, Johns Hopkins University School of Medicine, Baltimore, Maryland 21205, E-mail: eglowat1@jhmi.edu or pfuchs1@jhmi.edu.

Cite as: eNeuro 2016; 10.1523/ENEURO.0078-16.2016

GluA2-containing AMPA receptors distinguish ribbon-associated from ribbon-less afferent contacts on rat cochlear hair cells

Abbreviated Title: Diversity of afferent contacts on outer hair cells

Rodrigo Martinez- Monedero[*2], Chang Liu[*1], Catherine Weisz[1,3], Pankhuri Vyas, Paul Albert Fuchs & Elisabeth Glowatzki

Department of Otolaryngology, Head and Neck Surgery, The Center for Hearing and Balance and the Center for Sensory Biology, Institute for Basic Biomedical Sciences, and the [1]Department of Neuroscience, The Johns Hopkins University School of Medicine, Baltimore, MD 21205 USA. [2]Current address: Broad Clinical Fellow. Department of Otolaryngology & USC Stem Cell Department, University of Southern California, Los Angeles, CA 90033-9080 USA. [3]Current address: Section on Neuronal Circuitry, National Institute for Deafness and other Communication Disorders, NIH, Bethesda, MD 20892 USA. [*]Co-first authors.

Author Contributions

Experimental work and analyses were conducted by R. M-M, C.L, C.W. and P.V. E.G. designed, and directed the work. P.F. helped discuss the work, edited and revised the manuscript. All authors contributed to and approved the manuscript. P. F. (submitting author).

Correspondence should be addressed to:

Elisabeth Glowatzki eglowat1@jhmi.edu
Paul Fuchs pfuchs1@jhmi.edu

Number of figures: 6
Number of tables: 1
Number of multimedia: 0
Number of words in Abstract: 138
Number of words in Significance statement 108
Number of words in Introduction: 544
Number of words in Discussion: 1294

Acknowledgements

We thank Dr. M. Pucak, PhD for assistance with confocal imaging.

Conflict of Interest: The authors declare no conflict of interest in execution or publication of this study.

Funding Sources:

Supported by NIDCD R01DC006476 to EG, NIDCD R01DC011741 to PF, NIDCD P30 DC005211 to the Center for Hearing and Balance, T32 DC000023 (CW) F31 DC010948 (CW), by NS050274, the Multiphoton Imaging Core grant to Hopkins Neuroscience, by the John Mitchell, Jr. Trust and by the David M. Rubenstein Fund for Hearing Research to Hopkins Otolaryngology-HNS. This report also was supported in part by the Intramural Research Program of the NIH, NIDCD (CW).

ABSTRACT (138 words)

Mechanosensory hair cells release glutamate at ribbon synapses to excite postsynaptic afferent neurons, via AMPA-type ionotropic glutamate receptors (GluAs). However, type II afferent neurons contacting outer hair cells in the mammalian cochlea were thought to differ in this respect, failing to show GluA immunolabeling and with many 'ribbonless' afferent contacts. Here it is shown that antibodies to the AMPA subunit GluA2 labeled afferent contacts below inner and outer hair cells in the rat cochlea, and that synaptic currents in type II afferents had AMPAR-specific pharmacology. Only half the postsynaptic densities of type II afferents that labelled for PSD95, Shank or Homer were associated with GluA2 immunopuncta or presynaptic ribbons, the 'empty slots' corresponding to 'ribbonless' contacts described previously. These results extend the universality of AMPA-ergic transmission by hair cells, and support the existence of silent afferent contacts.

SIGNIFICANCE (108 words)

Transmission from cochlear hair cells to afferent neurons is mediated by ionotropic glutamate receptors. Inner hair cells efficiently drive acoustic coding in type I afferents that express GluA2-containing AMPA receptors. Type II cochlear afferents differ from type I afferents not only in number, caliber, myelination and excitability, but also in the utility of their terminal contacts with hair cells. Outer hair cell to type II afferent transmission is far less effective, but also employs GluA2-containing receptors. Only half the type II afferent boutons that immuno-labeled for postsynaptic density proteins had GluA2 receptors. And, only GluA2-containing

64 contacts were associated with presynaptic ribbons, the hair cell's transmitter release active
65 zones.
66
67 **INTRODUCTION (544 words)**
68 Mechanosensory hair cells of vertebrates release glutamate to excite afferent neurons. This
69 holds true as well within the mammalian cochlea where acoustic information is transmitted
70 from inner hair cells (IHC) to the predominant (95%) myelinated type I afferents by the
71 activation of AMPA-type receptors - AMPARs (Glowatzki and Fuchs, 2002; Ruel et al., 2000).
72 The fewer, smaller caliber, unmyelinated type II afferents contact many outer hair cells (OHC),
73 but are only weakly activated by glutamate release at those connections (Weisz et al., 2012).
74 Physiological studies suggest that AMPARs also mediate OHC transmission to type II afferents
75 (Weisz et al., 2009) although this result runs counter to the conclusion based on
76 immunolabeling that OHC synapses are not AMPAR-dependent (Liberman et al., 2011;
77 Matsubara et al., 1999; Ottersen et al., 1998). Synaptic signaling from OHCs to type II afferents
78 is further complicated by the presence of 'ribbonless' contacts (Dunn and Morest, 1975;
79 Liberman et al., 1990), and the expression of kainate receptors at both ribbon-containing and
80 ribbonless contacts (Fujikawa et al., 2014). Given these discrepancies and unknowns, it was of
81 interest to explore further the pharmacology of postsynaptic currents, to characterize the
82 distribution of postsynaptic proteins at the OHC to type II afferent contacts, and to compare
83 these to the better-characterized IHC to type I contact.
84 In mammals, heteromeric AMPA receptors are made of four different subunits, GluA1-4,
85 encoded by separate but related genes (Borges and Dingledine, 1998; Kohler et al., 1994).

Previous attempts with antibodies to the GluA2/3 heteromer failed to label type II contacts onto OHCs (Eybalin et al., 2004; Knipper et al., 1997; Liberman et al., 2011; Matsubara et al., 1996a; Meyer et al., 2009). More recently, antibodies specific for the GluA2 subunit showed specific labeling beneath inner, but not OHCs of adult mice (Fernandez et al., 2015; Fujikawa et al., 2014; Liberman et al., 2015). In contrast, the present work found GluA2 immunoreactivity in association with ribbon synapses of inner and outer hair cells of adult and young rats. Consistent with that result, glutamatergic synaptic currents in type II afferents of young rats were blocked by the AMPAR-specific antagonist CP-465,022 (Balannik et al., 2005; Lazzaro et al., 2002).

The organization of afferent synapses also was analyzed by immunolabel against postsynaptic density proteins. PSD-95, a PDZ-domain containing protein of the MAGUK (membrane-associated guanylate kinase) family is a ubiquitous component of glutamatergic synapses, including those of cochlear hair cells (Davies et al., 2001). Shank proteins interconnect many components of the postsynaptic density with the cytoskeletal matrix (Sheng and Kim, 2000), including NMDA, AMPA, and mGluRs; this last through the coupling protein Homer (Boeckers, 2006). In the present work antibodies to PSD-95, Shank and Homer were used to map their distribution under IHC and OHC. Consistent with previous reports (Liberman et al., 2011; Meyer et al., 2009; Wang and Green, 2011) the majority of postsynaptic densities in type I afferents beneath IHC were associated with GluA-positive immunopuncta and presynaptic ribbons. Beneath OHC however, only GluA2-containing postsynaptic densities (about half the total) were juxtaposed to presynaptic ribbons. The GluA2-lacking and ribbon-lacking postsynaptic densities are reminiscent of 'ribbonless' afferent contacts described by

108 others (Dunn and Morest, 1975; Liberman et al., 1990; Nadol, 1983) and may indicate that type
109 II afferents possess a type of 'silent synapse' that could be activated in response to changing
110 conditions.
111
112 **MATERIALS AND METHODS**
113 Adult or 1-2 week old Sprague Dawley albino rats of either sex (CD IGS rats, Charles River
114 Laboratories) were deeply anesthetized by isoflurane inhalation, decapitated, and the temporal
115 bone quickly removed. All experimental procedures involving animals were approved by the
116 [Authors' University] Animal Care and Use Committee.
117
118 *Immunohistochemistry.*
119 After removing the inner ear from the skull, a small hole was made in the apical bone of the
120 cochlea, to allow flow of solution. For fixation of the tissue, 4% paraformaldehyde (Electron
121 Microscopy Sciences) prepared in phosphate buffer solution (1x PBS), pH 7.4, was perfused
122 through the round and oval windows into the cochlea and the tissue was kept in fixative for 30
123 min to 2 hours at 4°C. After three washes in PBS, cochlear tissue was micro-dissected and freed
124 from bone to facilitate better access of the antibodies to the tissue. In a typical experiment,
125 cochlear tissue from 2 ears, 3 pieces per ear, were processed together. The tissue pieces were
126 transferred with a spoon into a drop of PBS located in the center region (about 1 cm in
127 diameter) of a microscope slide. Next, whole-mount preparations were incubated in a
128 permeabilizing solution with 0.5% of NP40 detergent in PBS for 10 to 60 minutes at 4°C. Tissue
129 was exposed to 1% bovine serum albumin (BSA) and 10% heat inactivated goat serum in PBS for

130 1 hour at room temperature (RT) to reduce non-specific labeling. Primary antibodies were
131 applied overnight at 4°C in 5% heat inactivated goat serum and 1% bovine serum albumin (BSA)
132 with or without 0.5% NP40 detergent depending on the antibody used.
133 The following primary antibodies were used: GluA2 monoclonal mouse antibody
134 (Chemicon #MAB397), GluA1 polyclonal rabbit antibody, GluA2N polyclonal rabbit antibody,
135 GluA3N polyclonal rabbit antibody and GluA4N polyclonal rabbit antibody (R. Huganir, Johns
136 Hopkins University School of Medicine, Baltimore, MD (Araki et al., 2010), CtBP2 rabbit
137 antibody (Bioworld Tech #BS2287), CtBP2 mouse antibody (BD #612044), Shank and Homer1
138 polyclonal antibodies (P. Worley, Johns Hopkins University School of Medicine), PSD95
139 polyclonal (BD Bioscience #610495) and PSD95 monoclonal (UC/Davis #73/028). After overnight
140 incubation with primary antibodies, samples were washed and incubated for 1 hour at room
141 temperature with the secondary antibodies. Alexa Fluor 488 goat anti-rabbit and Alexa Fluor
142 568 goat anti-mouse (Invitrogen), centrifuged at high speed and diluted at 1:1000 in 1xPBS,
143 were used as secondary antibodies. Samples were rinsed three times for 10 min each in PBS at
144 RT before mounting and viewing.
145
146 *Controls.*
147 The specificity of GluA2 antibodies was confirmed in control experiments on GluA2 null mice.
148 GluA2-null heterozygotes (Huganir laboratory, Neuroscience department, Johns Hopkins
149 University) were bred to provide homozygous null mice; genotype confirmed by polymerase
150 chain reaction. Tissue was fixed and immunolabeled using the same procedure as for
151 experimental animals. In three GluA2 null mice there was good labeling of presynaptic ribbons

with the antibody against CtBP2 in both OHCs and IHCs, but no GluA2 label. Wildtype littermates had positive CtBP2 and GluA2 label in the IHC area.

Secondary antibody controls.

This work was designed to address synaptic structure and location at the cellular level, rather than the sub-micron distribution of each protein component. Thus, simultaneous label with pre- and postsynaptic markers could present significant overlap in *z*-scan confocal microscopy and was the desired goal of this work; to evaluate the regional co-localization of a variety of postsynaptic proteins. However, this raised the question of whether such overlap represents true co-localization, or results from crosstalk between channels for the different fluorophores (Alexa fluor 488 and 568) that were conjugated to secondary antibodies. Thus some samples were incubated with only one primary antibody (e.g., CtBP2 antibody without GluA2 antibody; GluA2 antibody without CtBP2 antibody) followed by incubation with both secondary antibodies presented together. In neither case was there co-localized signal for the absent primary antibody.

Intracellular recording from type II cochlear afferents.

The apical turn of the cochlea was dissected from young rats (P7-P9), followed by the removal of stria vascularis and tectorial membrane. The cochlear turn was then secured onto a coverslip by an insect pin serving as a spring clamp and imaged under a microscope (Carl Zeiss Examiner D1) using a 40× water-immersion objective and a camera with contrast enhancement (Hamamatsu C2400-62). Three-to-four OHCs were removed with a glass suction pipette to

expose the dendrites of type II cochlear afferents. Extracellular solution contained (in mM): 5.8 KCl, 144 NaCl, 1.3 $CaCl_2$, 0.9 $MgCl_2$, 0.7 NaH_2PO4, 5 glucose, 10 HEPES, pH 7.4. Giga-ohm seal pipettes were pulled from 1mm borosilicate glass (WPI) with a final pipette resistance of 7-9 MΩ after fire-polish, and filled with intracellular solution containing (in mM): 110 K-methane sulfonate, 20 KCl, 0.1 $CaCl_2$, 3.5 $MgCl_2$, 5 K-EGTA, 5 HEPES, 5 Na_2phosphocreatine, 0.3 Tris-GTP, pH 7.2. Junction potentials (10 mV) for this solution were corrected in the reported membrane potential. The series resistance was less than 30 MΩ (membrane test of the pCLAMP 10.3 software - Molecular Devices) and was not corrected for the small currents recorded here. Intracellular recording from type II afferents was confirmed by the characteristic voltage gated currents elicited by a series of voltage steps and the presence of rapid synaptic currents. The frequency of 'spontaneous' synaptic currents was increased by bathing the tissue in 40 mM potassium saline (substituted for sodium) to depolarize hair cells. Synaptic events were collected for at least one minute prior to addition of the AMPAR antagonist CP-465,022 to the high potassium perfusate via a large bore application pipette positioned close to the recording site. All reagents were obtained from Sigma, except for philanthotoxin and CP-465,022 which were from Tocris.

Recordings (at room temperature) were made with a MultiClamp 700B amplifier and a Digidata 1440A (Molecular Devices), controlled by pCLAMP 10.3 software (Molecular Devices), sampled at 25 kHz and low-pass filtered at 1 – 10 kHz. Data were analyzed in Clampex (Molecular Devices) and Origin 9.0 (Origin Labs). EPSCs were selected and analyzed using MiniAnalysis software (Synaptosoft) with an amplitude criterion three times the root mean square of the noise.

196

197 *Type II fiber biocytin filling and peroxidase reaction for immunohistochemistry and detection of*
198 *labeling.*

199 0.3% biocytin (3.0mg/mL) was added to the intracellular solution of the patch pipettes for
200 delivery into type II afferents via whole-fiber tight-seal recordings. The tracer was detected
201 *post-hoc* using streptavidin-conjugated horseradish peroxidase, or streptavidin-conjugated
202 fluorescent labeling. In some experiments, the cochlear tissue was preloaded (30 second, room
203 temperature) with 5µM FM1-43FX (Invitrogen), a fluorescent dye that rapidly enters through
204 mechanotransduction channels and partitions into the hair cell membrane. Cochlear explants
205 with filled type II afferents were fixed immediately after recordings in 4% paraformaldehyde
206 (vol/vol) overnight at 4°C. After wash in PBS, the tissue was quenched in 10% H_2O_2 (in 10%
207 methanol and 90% PBS) for 10 minutes, then permeabilized in 2% Triton in PBS for 1 hour at
208 room temperature. Avidin/biotin complex (Vectastain ABC kit, Vector Labs) was added and the
209 tissue was incubated overnight at 4°C. Under a dissection microscope (Leica MS5), each
210 individual tissue was reacted with a diaminobenzidine-based peroxide substrate (ImmPACT DAB,
211 Vector) for about 10 minutes, until the cell and its arborization were visible. The tissue was then
212 transferred and mounted onto a microscope slide.

213 A second set of experiments combined fluorescent labeling of the fiber (biocytin,
214 streptavidin AF488) with immuno-fluorescent labeling of OHCs. The tissue with the filled type II
215 afferent fiber was fixed in 4 % PFA for 10-60 minutes at 4°C. Then the tissue was exposed to 1%
216 BSA and 10% heat inactivated goat serum in phosphate-buffered saline (PBS) for 1 hour at RT to
217 reduce non-specific labeling. Streptavidin-Alexa Fluor 488 conjugate and CtBP2 or PSD95

antibodies were applied overnight at 4°C in 5% heat inactivated goat serum and 1% BSA. Samples were washed and incubated for 1 hour at room temperature (RT) with the secondary antibodies Alexa Fluor 568 goat anti-rabbit and Alexa Fluor 633 goat anti-mouse (Invitrogen). Secondary antibodies were centrifuged at high speed and diluted at 1:1000 in 1 x PBS before use. Samples were rinsed three times for 10 min each in PBS at RT before mounting and viewing.

Image acquisition.

Mounted cochlear turns were imaged using a confocal laser-scanning microscope (Zeiss LSM 510 Meta) with appropriate excitation and emission filters. A Plan-Apochromat 100x oil objective N.A. 1.4 was used. Whole mount preparations of the apex-middle region of the adult (more than two months old) rat cochlea were used unless otherwise specified. For every experimental condition, cochlear turns of rats from at least 3 different litters were analyzed. From every organ of Corti, Z-stack projections were taken from at least three areas in the lower apex-upper middle turn of the organ of Corti. Analysis was focused on the endings of the type I and type II spiral ganglion afferent fibers that innervate inner and outer hair cells (IHCs and OHCs), respectively and each stack contained the entire synaptic pole of the hair cells as viewed from the endolymphatic surface of the organ of Corti. Each acquisition frame covered about 24 OHCs, and about 5 IHCs (visualized by CtBP2 immunoreactivity in nuclei, or background fluorescence in other experiments). The confocal detection volumes of all image channels were equalized simultaneously. Images were taken with sequential scanning with multitrack acquisition to reduce crosstalk. Care was taken to minimize pixel saturation in each image stack.

For morphological analysis stacks of confocal images (0.37 µm maximum *z*-intervals) were imported into Imaris XT software 7.4 (from LSM 510 Image acquisition) for 3D reconstruction and quantification.

3-D morphometry, puncta quantification and juxtaposition.

All quantitative analysis was performed with Imaris XT software (version 7.4) using raw image stacks, without any deconvolution, filtering, gamma correction or re-sampling. Antibody labeling occurred in discrete patches, or puncta at the base of the hair cells. The total number of synaptic markers was counted in each stack and divided by the number of hair cells. To evaluate juxtaposition between CtBP2, GluA2, PSD95, Shank and Homer immunolabel, an iso-surface of each signal was created in independent color channels. Puncta volumes were computed using functions that provide 3-D rendering and visualization of iso-surfaces enveloping all pixel clusters with intensities greater than a user–defined criterion value (and with greater than a minimum number of enveloped pixels). Puncta volumes were computed along the *x, y* and *z* coordinates of their centers. Surface to surface measurements were used to create a distance transformation channel with an intensity minimum representing the closest distance between two objects. A threshold was set at 0.5 µm or less to define juxtaposition of two different puncta. The computed results were corroborated by visual inspection of the puncta. Significance was measured using the Student's *t* test or one-way ANOVA test followed by the Bonferroni's multiple comparison test. All data are reported as mean ± standard error of the mean (SEM) unless otherwise noted. GraphPad Prism4 was used to compute statistical results.

Results

Relationship of presynaptic ribbons and postsynaptic GluA2 clusters at IHC and OHC afferent contacts.

In initial experiments, antibodies specific to each of the AMPAR subunits, GluA1-4, as well as that to the GluA2/3 combination were applied to excised adult rat cochlear whole-mounts (upper apical to middle turns). Among these, only anti-GluA2 produced localized, punctate labeling below OHCs in the rat cochlea. A monoclonal mouse antibody and a polyclonal rabbit antibody provided comparable results and so the resulting data were pooled for analysis and interpretation (see Methods). Double labeling with an antibody against CtBP2/RIBEYE (Lenzi and von Gersdorff, 2001; Schmitz et al., 2000; Wagner, 1997; Zenisek et al., 2003), was performed to relate postsynaptic GluA2 labeling to the location of presynaptic ribbons in hair cells (Fig. 1). With this combined labeling, both OHC and IHC afferent synapses were investigated in organs of Corti of the adult rat (2 months and older). The total number of puncta labeled by synaptic markers was counted in each *z*-stack and divided by the number of hair cells. Hair cells were enumerated separately by background fluorescence of cell bodies at high light intensity, or by labeling of their nuclei with the CtBP2/RIBEYE antibodies.

The average number of GluA2 puncta per OHC was 2.3 ± 0.2 and the number of CtBP2 puncta per OHC was 2.4 ± 0.1 (n = 72 OHCs analyzed from 3 experiments) (Fig. 1C). CtBP2 and GluA2 puncta were closely aligned in most cases (Fig. 1A, magnified inset). A juxtaposed CtBP2 punctum was present at 94.9 ± 1.1% of GluA2 puncta, and 85.5 ± 5.5% of CtBP2 puncta had an

associated GluA2 punctum (Fig.1C). Assuming that the GluA2 puncta represent functional synapses, this high level of juxtaposition suggests that AMPAR-mediated synaptic transmission occurs at ribbon synapses of OHCs, with 2-3 such ribbon synapses per OHC. The relationship of GluA2 and CtBP2 immunolabel was examined further by rotating the original Z-axis confocal stack into the Z-X and Z-Y planes (Fig. 1A). From these viewpoints the separation of red (CtBP2/RIBEYE) and green (GluA2) was better resolved.

In keeping with their known synaptic organization (middle cochlear turn), many more presynaptic ribbons and postsynaptic GluA2 receptor clusters were found among IHCs (Fig.1B). At individual IHCs there were 23.3 ± 0.6 GluA2 puncta and 22.4 ± 1.0 CtBP2 puncta (n = 50 IHCs from 9 experiments) (Fig 1D). CtBP2-labeled ribbons and GluA2 puncta were consistently juxtaposed (Fig. 1B, magnified inset). For 96.8 ± 1.0% of CtBP2 puncta, a juxtaposed GluA2 punctum was found and for 96.6 ± 1.1% of GluA2 puncta, a juxtaposed CtBP2 punctum was found (Fig.1D). These results with GluA2 labeling echo previous reports regarding the number of synapses per IHC and the close correspondence between CtBP2-labeled ribbons and GluA2/3 or GluA2 receptor clusters (Beutner and Moser, 2001; Brandt et al., 2003; Fuchs et al., 2003; Khimich et al., 2005; Liberman et al., 2011; Meyer et al., 2009; Neef et al., 2007). The separation of presynaptic CtBP2 and postsynaptic GluA2 puncta was better resolved in Z-stacks of the IHCs than in OHCs. This is probably due to a more-horizontal disposition of IHCs in cochlear whole mounts, so synaptic labeling was viewed with the higher resolution of the X-Y image plane. This is in contrast to vertically-oriented OHCs where pre- and post-synaptic elements appear to overlap in Z, but could be better separated in the X- or Y-axis.

306 The identity of neurotransmitter and receptors at the OHC to type II contact has been
307 debated for some years. The absence of GluR2/3 immunoreactivity led to the logical conclusion
308 that some mechanism other than AMPAR-mediated transmission operated there (Matsubara et
309 al., 1996a; Thiers et al., 2008). Initial studies of synaptic currents in type II afferents showed
310 that these were blocked by the non-selective AMPA/kainate antagonist NBQX (Weisz et al.,
311 2009), leaving open the possibility that postsynaptic kainate receptors respond to glutamate
312 release from OHCs (Fujikawa et al., 2014). Further support for the involvement of GluA2-
313 containing AMPA receptors was obtained by intracellular recording from type II afferents in
314 excised apical turns of young rat cochleas (P9). The highly potent AMPA-specific antagonist CP-
315 465,022 (Balannik et al., 2005; Lazzaro et al., 2002) was applied while recording potassium-
316 evoked excitatory post-synaptic currents (EPSCs – Fig 2A.). At 10 μM (3 fibers) and 100 μM (2
317 fibers) CP-465,022 completely eliminated EPSCs. Successive application of 1 μM, then 10 μM
318 CP-465,022 reduced EPSC amplitudes (Fig 2A, 2B) going from partial to complete block,
319 consistent with the reported potency of the drug on AMPA receptors (Lazzaro et al., 2002). At
320 1 μM CP-465,022 reduced the average EPSC amplitude by approximately 50% (Fig. 2C). To
321 further probe for kainate or other non-AMPA receptors, the amplitude of the residual current
322 in CP-465,022 was normalized to the control amplitude and its waveform compared to that
323 before block. There was no difference in waveform before and during block by CP-465,022 (Fig.
324 2D), although kainate receptor-mediated EPSCs have much slower kinetics than those served by
325 AMPA receptors at CNS synapses (Lerma and Marques, 2013). Thus if CP-resistant kainate
326 receptors do contribute to synaptic currents in type II afferents they were indistinguishable by
327 kinetics or sensitivity to CP-465,022.

328 Inclusion of the GluA2 subunit renders AMPARs impermeable to calcium (Hollmann et
329 al., 1991; Mishina et al., 1991), requiring that synaptic currents in type II afferents should flow
330 through calcium-impermeant channels if mediated by GluA2-containing AMPARs. This
331 suggestion can be tested by examining the effects of intracellular spermine. This polyamine
332 generates a voltage-dependent block of calcium-permeant glutamate receptors (i.e. non-GluA2-
333 containing), resulting in a sharply rectified current-voltage relation (Donevan and Rogawski,
334 1995). So the absence of rectification with intracellular spermine indicates the presence of
335 calcium impermeant GluA2 subunits. The voltage-dependence of EPSCs in six type II fibers
336 treated with intracellular spermine (100 µM) did not differ from control (exemplar in Fig. 3A, B),
337 consistent with low calcium permeability and the presence of GluA2 subunits. EPSCs in type II
338 fibers also were unaffected by the compounds philanthotoxin (Toth and McBain, 1998) and
339 Naspm (1-naphthyl acetyl spermine) (Tsubokawa et al., 1995) that act as channel blockers of
340 non-GluA2-containing receptors. Neither philanthotoxin (20 µM, 5 fibers), nor Naspm (10 µM,
341 5 fibers) altered the average amplitude of EPSCs in type II fibers (exemplars in Fig 3C, D).
342 Taken together with specific GluA2 immunolabeling in adult tissue (Fig. 1), these
343 indicators and the sensitivity to CP-465,022 support the conclusion that, as for the IHC to type I
344 synapse, GluA2-containing AMPARs mediate rapid glutamatergic excitation at the OHC to type
345 II afferent synapse in the rat cochlea. If other receptor types participate, their involvement is
346 indistinguishable from that of AMPARs in these recordings.
347
348 **Relationship of presynaptic ribbons and postsynaptic density proteins at IHC and OHC**
349 **afferent contacts.**

Further insight into the synaptic arrangements of type I and type II afferent neurons was gained using antibodies directed against postsynaptic density proteins PSD95, Shank and Homer. These antibodies were applied to cochlear whole mounts and their labeling compared to that of GluA2 clusters and presynaptic ribbons at both inner and outer hair cell afferent contacts. In the central nervous system, PSD95 participates in synaptic targeting of AMPA receptors through the coupling protein Stargazin and related transmembrane AMPA receptor regulatory proteins (TARPs) (Colledge et al., 2000; El-Husseini et al., 2000; Harms and Craig, 2005; Hirbec et al., 2003; Ives et al., 2004; Naisbitt et al., 1997; Sheng, 1997). PSD95 binding partners also include NMDA receptors (Boeckers, 2006). In contrast to the near membrane location of PSD95, the postsynaptic density organizing protein Shank extends further into the cytoplasm to link glutamate receptor activity and local cytoskeletal remodeling, particularly within actin-rich dendritic spines (Brandstatter et al., 2004). Shank also interacts with metabotropic glutamate receptors through the connecting protein Homer. The distribution of Shank and Homer was compared to that of PSD95 and to the presynaptic ribbon marker, CtBP2, at afferent contacts on IHCs in separate experiments.

The number of PSD95 puncta per IHC in the adult rat cochlea was 25.8 ± 0.7 and the number of CtBP2/RIBEYE puncta was 22.4 ± 1.0 in double labeling experiments (n = 60 IHCs in 5 mid-turn cochlear coils) (Fig. 4C, F). Both Shank and Homer antibodies labeled type I boutons beneath IHCs in a pattern that closely corresponded with PSD95 immunoreactivity (Fig. 4A, B). When comparing the number of puncta per IHC for CtBP2/RIBEYE, GluA2, PSD95, Shank and Homer, no significant differences were found (one way-ANOVA, $p = 0.117$), with all markers providing 21 to 26 puncta per IHC; PSD95 the most and Homer the least (Fig 4F). For more than

372 90% of Shank puncta (94.6 ± 1.1 %) (7 cochlear segments) and Homer puncta (90.4 ± 5.8 %) (3
373 cochlear segments), PSD95 was located within 0.5 µm, suggesting that Homer and Shank are
374 consistently expressed at postsynaptic densities of type I afferents (Fig. 4G). Likewise, Shank
375 was largely associated with PSD95 (Shank/PSD95 87.4 ± 2.4 %). The difference in numbers per
376 hair cell may help explain the observation that most Homer puncta were juxtaposed with
377 PSD95, however some PSD95 puncta did not appear to be juxtaposed to Homer (70.5 ± 11.2 %
378 of Homer/PSD95 (Fig. 4G)). This may reflect a lower signal to noise for Homer immunolabel, or
379 suggest a real difference in expression among type I boutons.
380 Presynaptic ribbons labeled with CtBP2/RIBEYE antibodies were almost always
381 juxtaposed to postsynaptic density proteins (Fig. 4H, 3 histogram bars on the left)
382 (PSD95/CTBP2: 93.1 ± 1.6%; 10 cochlear segments); (Shank/CtBP2: 89.9 ± 4.0%; 3 cochlear
383 segments); (Homer/CtBP2: 81.9 ± 2.7; 5 cochlear segments). Although not statistically
384 significant and so to be interpreted cautiously, the data might suggest that a minority of
385 postsynaptic density puncta were not within the 0.5 µm surface-to-surface distance of CtBP2-
386 immunolabled ribbons that was the criterion for juxtaposition. This fraction was larger for
387 Homer than for Shank, than for PSD95 respectively (Fig. 4H, 3 histogram bars on the right)
388 (CTBP2/PSD95: 78.9 ± 3.1 %); (CtBP2/Shank: 70.8 ± 4.3 %;); (CtBP2/Homer: 61.3 ± 10.6 %). The
389 average surface-to-surface distance between CtBP2/RIBEYE puncta and Homer puncta was
390 larger (0.05 ± 0.01 µm) than that for Shank (0.03 ± 0.01 µm) or PSD95 (0.03 ± 0.01 µm),
391 although not statistically significant (one way-ANOVA; $p > 0.05$). The significant observation is
392 that every IHC had similar numbers of all immunopuncta. Thus a majority of afferent contacts

393 on IHCs included the presynaptic ribbon, postsynaptic density proteins, and GluA2-containing
394 AMPARs. This was not the case for OHCs.
395
396 **Postsynaptic density proteins at OHC afferent contacts.**
397
398 Having established the presence of Shank and Homer immunolabel at IHC afferent
399 contacts, the distribution of immunolabel with those same antibodies was examined at the OHC
400 afferent contacts. In contrast to the individual discrete puncta observed beneath IHCs, PSD95,
401 Shank and Homer revealed more complex patterns that could extend several microns along the
402 synaptic pole of the OHC. These appeared as an irregular cluster or as an interconnected series,
403 like a short pearl chain (Fig. 5A, B, C, D, F, G). Postsynaptic densities beneath OHCs identified by
404 PSD95 immunolabel were also positive for Shank in double label experiments (Fig. 5A, insets).
405 Homer was not tested in a co-labeling experiment with other postsynaptic density markers, but
406 showed the same 'pearl chain' pattern as did PSD95 and Shank (Fig. 5D). The number of
407 postsynaptic density protein puncta per outer hair cell (PSD95: 4.5 ± 0.2; Shank: 4.2 ± 0.1;
408 Homer: 4.3 ± 0.5) was nearly twice the number of CtBP2 (2.4 ± 0.1) or GluA2 puncta (2.3 ± 0.2)
409 (one way-ANOVA, p = 0.01; Bonferroni's multiple comparison test; n = 72-168 OHCs in 3-7
410 cochlear segments) (Fig. 5E). This contrasts markedly with the equal numbers of these
411 components per each IHC.
412 The pattern of postsynaptic density markers had an interesting relationship to the
413 CtBP2-labeled presynaptic ribbons, as shown here for Shank (Fig. 5B, F). Most CtBP2-positive
414 ribbons were juxtaposed to Shank (84.9 ± 5.7%), PSD95 (90.6 ± 1.9%) and Homer (81.9 ± 6.2%)

(Fig. 5H). However, roughly half of the postsynaptic densities were 'ribbonless' with no associated CtBP2 puncta. Only 52.1 ± 1.9% of the Shank puncta, 49.2 ± 5.3% of PSD95 and 45.6 ± 2.3% of Homer had juxtaposed CtBP2 puncta. The percentages of PSD95, Shank or Homer puncta juxtaposed to CTBP2 were significantly lower than the percentage of CTBP2 puncta juxtaposed to the postsynaptic density proteins (one way-ANOVA test; $p \leq 0.01$; Bonferroni's multiple comparison test; Fig. 5H).

These statistics and the strong correspondence between GluA2 immuno-clusters and ribbons labeled with anti-CtBP2 (Fig. 1) suggest that GluA2 clusters might show a similar relationship to postsynaptic density proteins as does CtBP2. Indeed, double label experiments with anti-GluA2 and anti-Shank revealed only partial correspondence, as found for anti-CtBP2 and anti-Shank (Fig. 5G). Thus the number of postsynaptic densities, as defined by PSD95, Shank and Homer immunolabeling, was twice that of the ribbon-associated clusters of GluA2 receptors in type II afferents. Most GluA2 puncta were juxtaposed to Shank puncta, however, close to the half of Shank puncta did not have juxtaposed GluA2 label (Fig. 5G). In other words, about half the type II postsynaptic contacts as defined by PSD95, Shank or Homer immunolabel may be 'empty slots', unable to mediate rapid glutamatergic transmission (Fig. 5I) since they are associated with neither GluA2-containing AMPARs, nor ribbons.

Type II fibers form a stereotyped pattern of OHC innervation.

How do the 'pearl chain' patterns of PSD immunolabel relate to the terminal arbors of individual type II fibers? These extend spiral dendrites that contact numerous OHCs (Berglund and Ryugo, 1987; Brown, 1987; Echteler, 1992; Ginzberg and Morest, 1983, 1984; Huang et al.,

437 2007; Koundakjian et al., 2007; Liberman et al., 1990; Perkins and Morest, 1975; Simmons and
438 Liberman, 1988a, b). To label the peripheral type II fibers and to understand their specific
439 connectivity with OHCs, giga-ohm-seal intracellular recording was used to fill type II fibers
440 under OHCs with biocytin in excised apical turns of cochleas from young rats (postnatal days P7
441 to P9). After streptavidin-peroxidase processing, 15 type II fibers were visualized and measured
442 from their somata in the spiral ganglion (white arrowhead Fig. 6A) to their basal-most endings
443 along the cochlear spiral. The peripheral neurite leaves the soma in the spiral ganglion to cross
444 the floor of the tunnel of Corti and turns ~ 90 degrees to travel toward the cochlear base along
445 the outer spiral bundle (Fig. 6A), sometimes switching between OHC rows (Fig. 6B). Over half
446 the filled fibers (8/15) had a single spiral process that averaged 714 ± 81 µm (n=8) from the
447 turning point to the basal-most tip (Table 1). An average of 17 ± 1.4 short branches off the
448 spiral process formed *en passant* (Fig. 6B, C red arrows) and terminal swellings (Fig 6B, C white
449 arrowheads). These terminal branches tended to cluster (12 ± 1 branches, spanning a distance
450 of 139 ± 19 µm (n=8)) with smaller secondary clusters 100 µm or more distant in some cases. In
451 one of the 8 'single process' fibers two synaptic zones 228 µm apart had nearly equal branching
452 (12 and 8 branches). The spiral dendrite also could split into 2 (6/15 fibers) or 3 (1 fiber)
453 basally-projecting processes (averaging 619 ± 73 µm in length). One such fiber branched as it
454 crossed the tunnel of Corti, and one fiber had branches extending both basally and apically.
455 Even including these exceptions, the overall length of the spiral process, the number of synaptic
456 branches and terminal arborization zones were similar among all 15 fibers (Table 1). The
457 number of branches within the terminal arbors of all the type II fibers averaged 16 ± 1.4 (n = 15).
458 These terminal branches had an average length of 10.9 ± 1.7 µm. Terminal branches had an

459 average of 2.0 ± 0.2 *en passant* swellings in addition to the terminal bouton. Each terminal
460 branch contacted 1-3 OHCs in the same row. The average total number of OHCs contacted by
461 each type II fiber was 23.7 ± 1.5. Some branches showed arching shapes (Fig. 6C, inset), that
462 could correspond to the 'pearl chain' postsynaptic densities described in Fig. 5. Although some
463 fibers split into two or three, in 5 of 7 such cases, terminal branches arose from only one of the
464 arbors, or prior to the branch point, so that all 15 fibers, whether possessing one or more major
465 processes, had similar numbers of terminal branches, and presumably equivalent numbers of
466 synaptic contacts.

467 The location of the main terminal arbor (synaptic input zone) ranged from 700 to 1600
468 µm (average 1167 ± 72 µm, n = 15) from the cochlear apex, placing the synaptic area in a
469 frequency range of ~ 9 kHz (Muller, 1991). On the other hand, the 90 degree turning point of
470 the fibers was located at 500 to 1000 µm (average 742 ± 55 µm, n = 15) from the apex, placing
471 it in the frequency range of 7 kHz. Thus, as noted previously (Brown, 1987), type II afferents, if
472 sufficiently sensitive, would report vibrations one quarter to one half octave higher in
473 frequency than type I afferents projecting in parallel to the same tonotopic zone of the cochlear
474 nucleus.

475 The number of fibers per OHC in the biocytin/streptavidin/peroxidase labeling was
476 determined by identifying labeled branches with a bright field microscope and counting
477 individual OHCs by shape and location. To verify these results, fluorescent labeling of the fiber
478 (biocytin, Streptavidin-Alexa Fluor 488) was combined with fluorescent labeling of OHCs. In one
479 set of experiments, OHC nuclei were counterstained with DAPI (Fig. 6C). In a second set of
480 experiments, the tissue was perfused with 5 µM FM1-43 for 30 s, a fluorescent dye that is taken

up by hair cells through the transduction channel (Nishikawa and Sasaki, 1996) (Fig. 6D). The main terminal zone of a filled fiber was investigated with confocal microscopy. Again, branching fibers and fibers with bouton endings and *en passant* swellings were visible and branches appeared to arc around the synaptic pole of the OHC (Fig. 6D, insets). In this dataset, the number of OHCs contacted by one fiber was 23 ± 2.2 (n = 9), identical to the result in preparations with unlabeled OHCs.

The combination of pre- or postsynaptic immunolabel with fiber filling was only occasionally successful. This may be a result of tissue condition after the time required for intracellular recording, and/or a reflection of less robust expression of synaptic proteins in the 8-10 day old animals needed for successful fiber recording. In any event even this low success rate provides qualitative, if not quantitative description. CtBP2 immunopuncta were located near to some, but not all terminal swellings of a filled fiber (Fig. 6E), reinforcing the possibility that type II fibers can form nonfunctional contacts with OHCs. Additional immunolabeling was carried out on young cochlear whole-mounts that were processed similarly to the adult tissues. Double-immunolabel for CtBP2 and PSD-95 gave an intermittent 'pearl chain' association like that onto adult OHCs (Fig. 6F).

DISCUSSION (1294 words)

Our understanding of synaptic transmission between hair cells and afferent neurons of the cochlea has advanced gradually (Defourny et al., 2011; Fuchs, 2005; Fuchs et al., 2003; Glowatzki et al., 2008; Guth et al., 1976; Hudspeth, 1997; Meyer and Moser, 2010; Ruel et al., 2007). Neuroanatomical studies led the way, with the description of two distinct classes of

503 neurons that differentially innervate inner and outer hair cells; type I afferents making single
504 contacts with single IHCs, type II afferents contacting 5-28 or more OHCs (Kiang et al., 1982;
505 Nadol, 1988; Ota and Kimura, 1980; Perkins and Morest, 1975; Pujol et al., 1978; Ruggero et al.,
506 1982; Spoendlin, 1975). Glutamatergic transmission from inner hair cells to type I afferents has
507 been well-accepted for many years (Bledsoe et al., 1981; Bobbin et al., 1991; Glowatzki and
508 Fuchs, 2002; Guth and Bobbin, 1971; Guth et al., 1976; Ottersen et al., 1998; Pujol et al., 1985),
509 but the same was firmly established for outer hair cells only with the advent of intracellular
510 recordings from type II fibers (Weisz et al., 2009; Weisz et al., 2012).

511 A remaining unknown was the identity of the glutamatergic receptor in type II afferents.
512 Antibodies to the GluA2/GluA3 AMPA receptor heteromer or to the GluA2 subunit reliably
513 labeled type I afferent contacts beneath inner hair cells, but failed to do so at the adult OHC-
514 type II connection in earlier studies (Eybalin et al., 2004; Fujikawa et al., 2014; Knipper et al.,
515 1997; Liberman et al., 2011; Matsubara et al., 1996b; Meyer et al., 2009). However, the present
516 work shows that GluA2-specific antibodies labelled postsynaptic receptor clusters beneath both
517 inner and outer hair cells of adult rats. Two different GluA2 antibodies gave the same result,
518 and failed to label contacts onto IHCs of GluA2-null mice. GluA2 receptors were found in
519 postsynaptic densities that co-localized with presynaptic ribbons in OHCs, but were absent from
520 postsynaptic densities that did not face presynaptic ribbons. Intracellular recordings from type
521 II afferents showed that synaptic currents were sensitive to the AMPA-selective antagonist CP-
522 465,022 and were carried by calcium-impermeant channels, consistent with inclusion of the
523 GluA2 subunit. Thus, biophysics, pharmacology and immunohistology support the conclusion
524 that AMPA-type receptors (GluA2-containing) mediate glutamatergic transmission from both

525 IHCs and OHCs onto their respective afferents. While electrophysiological evidence comes only
526 from apical segments of the young rat, immunolabeling for GluA2 below OHCs was found in
527 middle turns of adult rat cochleas, supporting the conclusion that AMPA receptors serve this
528 synapse throughout life. The presence of GluA2 does not rule out the participation of other
529 components, such as kainate receptors (Fujikawa et al., 2014; Peppi et al., 2012), but their
530 contribution is either undetectable in these recordings, or indistinguishable from that of AMPA-
531 type receptors. It will be of interest to determine whether more subtle modulatory effects
532 might depend on kainate receptor activity.

533 Type I and type II afferents differ in morphology, cochlear innervation pattern, synaptic
534 transfer function, and resistance to acoustic trauma. These differences might be reflected in, or
535 even dependent upon, the molecular composition of their synaptic contacts. GluA2
536 immunolabeling seemed generally fainter in type II than type I dendrites, perhaps indicating a
537 lower density of receptors in each cluster. However, the chief distinction was that the
538 postsynaptic densities of type II afferents (defined by immunopuncta of any of PSD95, Shank or
539 Homer) are more numerous than the GluA2 clusters immediately opposite synaptic ribbons of
540 the outer hair cell; in contrast to the equal numbers of receptor clusters, ribbons and
541 postsynaptic densities at the IHC to type I contacts. This difference may reflect in part the
542 structure of the afferent ending itself. Type I afferents terminate in single small, unbranched
543 boutons opposite IHC ribbons. In contrast, type II afferents extend hundreds of microns along
544 the outer hair cell rows and form functional synapses with at least ten, and probably many
545 more OHCs (Berglund and Ryugo, 1987; Brown, 1987; Fechner et al., 2001; Ginzberg and
546 Morest, 1983; Jagger and Housley, 2003; Nayagam et al., 2011; Perkins and Morest, 1975;

Simmons and Liberman, 1988a; Weisz et al., 2012). The area of contact with the OHC has been described as a discrete bouton in some studies (Ginzberg and Morest, 1984; Nadol, 1983), but can be more extensive, forming *en passant* synapses as it travels past the OHC (Francis and Nadol, 1993; Nadol, 1988; Sobkowicz et al., 1993). The 'pearl chain' pattern observed here with PSD95, Shank or Homer immunolabel is consistent with this description of *en passant* as well as terminal contacts with OHCs and corresponds with the 'C-shape' pattern described previously (Fujikawa et al., 2014). GluA2 immunopuncta align with only a subset of postsynaptic densities in a pearl chain, but are closely correspondent with presynaptic ribbons. Thus, some postsynaptic densities of type II neurons appear to be 'empty slots', without GluA2 receptors, and lacking presynaptic ribbons.

We conclude that AMPA-mediated synaptic currents result from vesicular glutamate released at ribbons facing GluA2-positive terminals of type II afferents. This leaves unresolved the question of what, if any, transmission also might occur at ribbonless contacts. Kainate receptors are found at ribbonless contacts of type II afferents onto rat OHCs (Fujikawa et al., 2014), but it remains to be determined what role they play. NMDA receptors have been implicated in the plasticity of afferent contacts on IHCs (Chen et al., 2009; d'Aldin et al., 1997; Knipper et al., 1997; Usami et al., 1995) but there is no evidence as yet for a role in type II afferents. Finally, Homer could provide an anchor for metabotropic glutamate receptors in cochlear afferents (Kleinlogel et al., 1999; Niedzielski et al., 1997; Peng et al., 2004; Safieddine and Eybalin, 1995). An experimental design that reveals longer-lasting, modulatory changes in excitability may be required to directly assess putative non-AMPAR inputs.

An intriguing proposition is that ribbonless contacts provide a reservoir of plasticity for the type II afferents – somewhat like 'silent synapses' found in the central nervous system (Kerchner and Nicoll, 2008), although requiring both presynaptic ribbons and postsynaptic AMPARs for activation. Long-term plasticity in the hippocampus results in part from the insertion of AMPA receptors into the postsynaptic density of previously silent synapses (Colledge et al., 2000; El-Husseini et al., 2000; Harms and Craig, 2005; Hirbec et al., 2003; Ives et al., 2004; Liao et al., 2001; Naisbitt et al., 1997; Petralia et al., 1999; Sheng, 1997). Several observations suggest that type II afferents may be able to adapt to changing cochlear conditions. First is that type II afferents are resistant to cochlear trauma, remaining even after OHC damage (Kujawa and Liberman, 2009; Ryan et al., 1980; Spoendlin, 1971). Second is that 'empty' PSDs could provide a substrate for enhanced transmission by the addition of GluA2 receptors (and presynaptic ribbons in the hair cell). Perhaps previously silent synapses 'awaken' to replace lost inputs, especially given the extensive arbors of type II afferents that could span the boundaries of damaged regions. Third, the numbers of afferent and efferent synapses are reciprocally related during the postnatal maturation of IHCs (Johnson et al., 2013; Katz et al., 2004; Roux et al., 2011), and efferent synapses return to the partially denervated IHCs of aged, deaf mice (Lauer et al., 2012; Zachary and Fuchs, 2015). Fourth, OHCs in mice with reduced or absent efferent function have more type II afferent contacts with ribbons than do wildtype OHCs (Fuchs et al., 2014; Pujol and Carlier, 1982), although other work failed to find this effect (Liberman et al., 2000). Type II afferents can be activated by cochlear tissue damage (Liu et al., 2015) which could serve as a trigger for activity-dependent enhancement of synaptic

589 connectivity. It will be of interest to examine the distribution of synaptic proteins in type II
590 afferents within, or spanning the boundaries of, regions of outer hair cell damage.
591
592
593 **References**

594 Araki, Y., Lin, D.T., and Huganir, R.L. (2010). Plasma membrane insertion of the AMPA
595 receptor GluA2 subunit is regulated by NSF binding and Q/R editing of the ion pore.
596 Proceedings of the National Academy of Sciences of the United States of America *107*, 11080-
597 11085.
598 Balannik, V., Menniti, F.S., Paternain, A.V., Lerma, J., and Stern-Bach, Y. (2005). Molecular
599 mechanism of AMPA receptor noncompetitive antagonism. Neuron *48*, 279-288.
600 Berglund, A.M., and Ryugo, D.K. (1987). Hair cell innervation by spiral ganglion neurons in the
601 mouse. The Journal of comparative neurology *255*, 560-570.
602 Beutner, D., and Moser, T. (2001). The presynaptic function of mouse cochlear inner hair cells
603 during development of hearing. J Neurosci *21*, 4593-4599.
604 Bledsoe, S.C., Jr., Bobbin, R.P., and Chihal, D.M. (1981). Kainic acid: an evaluation of its action
605 on cochlear potentials. Hear Res *4*, 109-120.
606 Bobbin, R.P., Ceasar, G., and Fallon, M. (1991). Changing cation levels (Mg2+, Ca2+, Na+)
607 alters the release of glutamate, GABA and other substances from the guinea pig cochlea. Hear
608 Res *54*, 135-144.
609 Boeckers, T.M. (2006). The postsynaptic density. Cell Tissue Res *326*, 409-422.
610 Borges, K., and Dingledine, R. (1998). AMPA receptors: molecular and functional diversity.
611 Progress in brain research *116*, 153-170.

612 Brandstatter, J.H., Dick, O., and Boeckers, T.M. (2004). The postsynaptic scaffold proteins
613 ProSAP1/Shank2 and Homer1 are associated with glutamate receptor complexes at rat retinal
614 synapses. J Comp Neurol *475*, 551-563.
615 Brandt, A., Striessnig, J., and Moser, T. (2003). CaV1.3 channels are essential for development
616 and presynaptic activity of cochlear inner hair cells. J Neurosci *23*, 10832-10840.
617 Brown, M.C. (1987). Morphology of labeled afferent fibers in the guinea pig cochlea. The
618 Journal of comparative neurology *260*, 591-604.
619 Chen, Z., Peppi, M., Kujawa, S.G., and Sewell, W.F. (2009). Regulated expression of surface
620 AMPA receptors reduces excitotoxicity in auditory neurons. Journal of neurophysiology *102*,
621 1152-1159.
622 Colledge, M., Dean, R.A., Scott, G.K., Langeberg, L.K., Huganir, R.L., and Scott, J.D. (2000).
623 Targeting of PKA to glutamate receptors through a MAGUK-AKAP complex. Neuron *27*, 107-
624 119.
625 d'Aldin, C.G., Ruel, J., Assie, R., Pujol, R., and Puel, J.L. (1997). Implication of NMDA type
626 glutamate receptors in neural regeneration and neoformation of synapses after excitotoxic injury
627 in the guinea pig cochlea. International journal of developmental neuroscience : the official
628 journal of the International Society for Developmental Neuroscience *15*, 619-629.
629 Davies, C., Tingley, D., Kachar, B., Wenthold, R.J., and Petralia, R.S. (2001). Distribution of
630 members of the PSD-95 family of MAGUK proteins at the synaptic region of inner and outer
631 hair cells of the guinea pig cochlea. Synapse (New York, NY *40*, 258-268.
632 Defourny, J., Lallemend, F., and Malgrange, B. (2011). Structure and development of cochlear
633 afferent innervation in mammals. Am J Physiol Cell Physiol *301*, C750-761.

634 Donevan, S.D., and Rogawski, M.A. (1995). Intracellular polyamines mediate inward
635 rectification of Ca(2+)-permeable alpha-amino-3-hydroxy-5-methyl-4-isoxazolepropionic acid
636 receptors. Proceedings of the National Academy of Sciences of the United States of America *92*,
637 9298-9302.
638 Dunn, R.A., and Morest, D.K. (1975). Receptor synapses without synaptic ribbons in the cochlea
639 of the cat. Proceedings of the National Academy of Sciences of the United States of America *72*,
640 3599-3603.
641 Echteler, S.M. (1992). Developmental segregation in the afferent projections to mammalian
642 auditory hair cells. Proc Natl Acad Sci U S A *89*, 6324-6327.
643 El-Husseini, A.E., Schnell, E., Chetkovich, D.M., Nicoll, R.A., and Bredt, D.S. (2000). PSD-95
644 involvement in maturation of excitatory synapses. Science *290*, 1364-1368.
645 Eybalin, M., Caicedo, A., Renard, N., Ruel, J., and Puel, J.L. (2004). Transient Ca2+-permeable
646 AMPA receptors in postnatal rat primary auditory neurons. The European journal of
647 neuroscience *20*, 2981-2989.
648 Fechner, F.P., Nadol, J.J., Burgess, B.J., and Brown, M.C. (2001). Innervation of supporting
649 cells in the apical turns of the guinea pig cochlea is from type II afferent fibers. The Journal of
650 comparative neurology *429*, 289-298.
651 Fernandez, K.A., Jeffers, P.W., Lall, K., Liberman, M.C., and Kujawa, S.G. (2015). Aging after
652 noise exposure: acceleration of cochlear synaptopathy in "recovered" ears. J Neurosci *35*, 7509-
653 7520.
654 Francis, H.W., and Nadol, J.B., Jr. (1993). Patterns of innervation of outer hair cells in a
655 chimpanzee: I. Afferent and reciprocal synapses. Hearing research *64*, 184-190.

656 Fuchs, P.A. (2005). Time and intensity coding at the hair cell's ribbon synapse. The Journal of
657 physiology *566*, 7-12.
658 Fuchs, P.A., Glowatzki, E., and Moser, T. (2003). The afferent synapse of cochlear hair cells.
659 Current opinion in neurobiology *13*, 452-458.
660 Fuchs, P.A., Lehar, M., and Hiel, H. (2014). Ultrastructure of cisternal synapses on outer hair
661 cells of the mouse cochlea. The Journal of comparative neurology *522*, 717-729.
662 Fujikawa, T., Petralia, R.S., Fitzgerald, T.S., Wang, Y.X., Millis, B., Morgado-Diaz, J.A.,
663 Kitamura, K., and Kachar, B. (2014). Localization of kainate receptors in inner and outer hair
664 cell synapses. Hearing research *314*, 20-32.
665 Ginzberg, R.D., and Morest, D.K. (1983). A study of cochlear innervation in the young cat with
666 the Golgi method. Hearing research *10*, 227-246.
667 Ginzberg, R.D., and Morest, D.K. (1984). Fine structure of cochlear innervation in the cat.
668 Hearing research *14*, 109-127.
669 Glowatzki, E., and Fuchs, P.A. (2002). Transmitter release at the hair cell ribbon synapse. Nature
670 neuroscience *5*, 147-154.
671 Glowatzki, E., Grant, L., and Fuchs, P. (2008). Hair cell afferent synapses. Current opinion in
672 neurobiology *18*, 389-395.
673 Guth, P.S., and Bobbin, R.P. (1971). The pharmacology of peripheral auditory processes;
674 cochlear pharmacology. Adv Pharmacol Chemother *9*, 93-130.
675 Guth, P.S., Norris, C.H., and Bobbin, R.P. (1976). The pharmacology of transmission in the
676 peripheral auditory system. Pharmacological reviews *28*, 95-125.
677 Harms, K.J., and Craig, A.M. (2005). Synapse composition and organization following chronic
678 activity blockade in cultured hippocampal neurons. J Comp Neurol *490*, 72-84.

679 Hirbec, H., Francis, J.C., Lauri, S.E., Braithwaite, S.P., Coussen, F., Mulle, C., Dev, K.K.,
680 Coutinho, V., Meyer, G., Isaac, J.T., *et al.* (2003). Rapid and differential regulation of AMPA
681 and kainate receptors at hippocampal mossy fibre synapses by PICK1 and GRIP. Neuron *37*,
682 625-638.
683 Hollmann, M., Hartley, M., and Heinemann, S. (1991). Ca2+ permeability of KA-AMPA--gated
684 glutamate receptor channels depends on subunit composition. Science *252*, 851-853.
685 Huang, L.C., Thorne, P.R., Housley, G.D., and Montgomery, J.M. (2007). Spatiotemporal
686 definition of neurite outgrowth, refinement and retraction in the developing mouse cochlea.
687 Development (Cambridge, England) *134*, 2925-2933.
688 Hudspeth, A.J. (1997). How hearing happens. Neuron *19*, 947-950.
689 Ives, J.H., Fung, S., Tiwari, P., Payne, H.L., and Thompson, C.L. (2004). Microtubule-associated
690 protein light chain 2 is a stargazin-AMPA receptor complex-interacting protein in vivo. J Biol
691 Chem *279*, 31002-31009.
692 Jagger, D.J., and Housley, G.D. (2003). Membrane properties of type II spiral ganglion neurones
693 identified in a neonatal rat cochlear slice. The Journal of physiology *552*, 525-533.
694 Johnson, S.L., Wedemeyer, C., Vetter, D.E., Adachi, R., Holley, M.C., Elgoyhen, A.B., and
695 Marcotti, W. (2013). Cholinergic efferent synaptic transmission regulates the maturation of
696 auditory hair cell ribbon synapses. Open biology *3*, 130163.
697 Katz, E., Elgoyhen, A.B., Gomez-Casati, M.E., Knipper, M., Vetter, D.E., Fuchs, P.A., and
698 Glowatzki, E. (2004). Developmental regulation of nicotinic synapses on cochlear inner hair
699 cells. J Neurosci *24*, 7814-7820.
700 Kerchner, G.A., and Nicoll, R.A. (2008). Silent synapses and the emergence of a postsynaptic
701 mechanism for LTP. Nature reviews Neuroscience *9*, 813-825.

Khimich, D., Nouvian, R., Pujol, R., Tom Dieck, S., Egner, A., Gundelfinger, E.D., and Moser, T. (2005). Hair cell synaptic ribbons are essential for synchronous auditory signalling. Nature *434*, 889-894.

Kiang, N.Y., Rho, J.M., Northrop, C.C., Liberman, M.C., and Ryugo, D.K. (1982). Hair-cell innervation by spiral ganglion cells in adult cats. Science (New York, NY *217*, 175-177.

Kleinlogel, S., Oestreicher, E., Arnold, T., Ehrenberger, K., and Felix, D. (1999). Metabotropic glutamate receptors group I are involved in cochlear neurotransmission. Neuroreport *10*, 1879-1882.

Knipper, M., Kopschall, I., Rohbock, K., Kopke, A.K., Bonk, I., Zimmermann, U., and Zenner, H. (1997). Transient expression of NMDA receptors during rearrangement of AMPA-receptor-expressing fibers in the developing inner ear. Cell and tissue research *287*, 23-41.

Kohler, M., Kornau, H.C., and Seeburg, P.H. (1994). The organization of the gene for the functionally dominant alpha-amino-3-hydroxy-5-methylisoxazole-4-propionic acid receptor subunit GluR-B. The Journal of biological chemistry *269*, 17367-17370.

Koundakjian, E.J., Appler, J.L., and Goodrich, L.V. (2007). Auditory neurons make stereotyped wiring decisions before maturation of their targets. J Neurosci *27*, 14078-14088.

Kujawa, S.G., and Liberman, M.C. (2009). Adding insult to injury: cochlear nerve degeneration after "temporary" noise-induced hearing loss. J Neurosci *29*, 14077-14085.

Lauer, A.M., Fuchs, P.A., Ryugo, D.K., and Francis, H.W. (2012). Efferent synapses return to inner hair cells in the aging cochlea. Neurobiology of aging *33*, 2892-2902.

Lazzaro, J.T., Paternain, A.V., Lerma, J., Chenard, B.L., Ewing, F.E., Huang, J., Welch, W.M., Ganong, A.H., and Menniti, F.S. (2002). Functional characterization of CP-465,022, a selective, noncompetitive AMPA receptor antagonist. Neuropharmacology *42*, 143-153.

725 Lenzi, D., and von Gersdorff, H. (2001). Structure suggests function: the case for synaptic
726 ribbons as exocytotic nanomachines. BioEssays : news and reviews in molecular, cellular and
727 developmental biology *23*, 831-840.
728 Lerma, J., and Marques, J.M. (2013). Kainate receptors in health and disease. Neuron *80*, 292-
729 311.
730 Liao, D., Scannevin, R.H., and Huganir, R. (2001). Activation of silent synapses by rapid
731 activity-dependent synaptic recruitment of AMPA receptors. J Neurosci *21*, 6008-6017.
732 Liberman, L.D., Suzuki, J., and Liberman, M.C. (2015). Dynamics of cochlear synaptopathy
733 after acoustic overexposure. J Assoc Res Otolaryngol *16*, 205-219.
734 Liberman, L.D., Wang, H., and Liberman, M.C. (2011). Opposing gradients of ribbon size and
735 AMPA receptor expression underlie sensitivity differences among cochlear-nerve/hair-cell
736 synapses. The Journal of neuroscience : the official journal of the Society for Neuroscience *31*,
737 801-808.
738 Liberman, M.C., Dodds, L.W., and Pierce, S. (1990). Afferent and efferent innervation of the cat
739 cochlea: quantitative analysis with light and electron microscopy. The Journal of comparative
740 neurology *301*, 443-460.
741 Liberman, M.C., O'Grady, D.F., Dodds, L.W., McGee, J., and Walsh, E.J. (2000). Afferent
742 innervation of outer and inner hair cells is normal in neonatally de-efferented cats. The Journal of
743 comparative neurology *423*, 132-139.
744 Liu, C., Glowatzki, E., and Fuchs, P.A. (2015). Unmyelinated type II afferent neurons report
745 cochlear damage. Proceedings of the National Academy of Sciences of the United States of
746 America.

747 Matsubara, A., Laake, J.H., Davanger, S., Usami, S., and Ottersen, O.P. (1996a). Organization of
748 AMPA receptor subunits at a glutamate synapse: A quantitative immunogold analysis of hair
749 cell synapses in the rat organ of Corti. J Neurosci *16*, 4457-4467.
750 Matsubara, A., Laake, J.H., Davanger, S., Usami, S., and Ottersen, O.P. (1996b). Organization of
751 AMPA receptor subunits at a glutamate synapse: a quantitative immunogold analysis of hair cell
752 synapses in the rat organ of Corti. J Neurosci *16*, 4457-4467.
753 Matsubara, A., Takumi, Y., Nakagawa, T., Usami, S., Shinkawa, H., and Ottersen, O.P. (1999).
754 Immunoelectron microscopy of AMPA receptor subunits reveals three types of putative
755 glutamatergic synapse in the rat vestibular end organs. Brain research *819*, 58-64.
756 Meyer, A.C., Frank, T., Khimich, D., Hoch, G., Riedel, D., Chapochnikov, N.M., Yarin, Y.M.,
757 Harke, B., Hell, S.W., Egner, A.*, et al.* (2009). Tuning of synapse number, structure and function
758 in the cochlea. Nature neuroscience *12*, 444-453.
759 Meyer, A.C., and Moser, T. (2010). Structure and function of cochlear afferent innervation.
760 Current opinion in otolaryngology & head and neck surgery *18*, 441-446.
761 Mishina, M., Sakimura, K., Mori, H., Kushiya, E., Harabayashi, M., Uchino, S., and Nagahari, K.
762 (1991). A single amino acid residue determines the Ca2+ permeability of AMPA-selective
763 glutamate receptor channels. Biochem Biophys Res Commun *180*, 813-821.
764 Muller, M. (1991). Developmental changes of frequency representation in the rat cochlea. Hear
765 Res *56*, 1-7.
766 Nadol, J.B., Jr. (1983). Serial section reconstruction of the neural poles of hair cells in the human
767 organ of Corti. II. outer hair cells. Laryngoscope *93*, 780-791.
768 Nadol, J.B., Jr. (1988). Comparative anatomy of the cochlea and auditory nerve in mammals.
769 Hearing research *34*, 253-266.

770 Naisbitt, S., Kim, E., Weinberg, R.J., Rao, A., Yang, F.C., Craig, A.M., and Sheng, M. (1997).
771 Characterization of guanylate kinase-associated protein, a postsynaptic density protein at
772 excitatory synapses that interacts directly with postsynaptic density-95/synapse-associated
773 protein 90. J Neurosci *17*, 5687-5696.
774 Nayagam, B.A., Muniak, M.A., and Ryugo, D.K. (2011). The spiral ganglion: connecting the
775 peripheral and central auditory systems. Hearing research *278*, 2-20.
776 Neef, A., Khimich, D., Pirih, P., Riedel, D., Wolf, F., and Moser, T. (2007). Probing the
777 mechanism of exocytosis at the hair cell ribbon synapse. J Neurosci *27*, 12933-12944.
778 Niedzielski, A.S., Safieddine, S., and Wenthold, R.J. (1997). Molecular analysis of excitatory
779 amino acid receptor expression in the cochlea. Audiology & neuro-otology *2*, 79-91.
780 Nishikawa, S., and Sasaki, F. (1996). Internalization of styryl dye FM1-43 in the hair cells of
781 lateral line organs in Xenopus larvae. J Histochem Cytochem *44*, 733-741.
782 Ota, C.Y., and Kimura, R.S. (1980). Ultrastructural study of the human spiral ganglion. Acta
783 Otolaryngol *89*, 53-62.
784 Ottersen, O.P., Takumi, Y., Matsubara, A., Landsend, A.S., Laake, J.H., and Usami, S. (1998).
785 Molecular organization of a type of peripheral glutamate synapse: the afferent synapses of hair
786 cells in the inner ear. Progress in neurobiology *54*, 127-148.
787 Peng, B.G., Li, Q.X., Ren, T.Y., Ahmad, S., Chen, S.P., Chen, P., and Lin, X. (2004). Group I
788 metabotropic glutamate receptors in spiral ganglion neurons contribute to excitatory
789 neurotransmissions in the cochlea. Neuroscience *123*, 221-230.
790 Peppi, M., Landa, M., and Sewell, W.F. (2012). Cochlear kainate receptors. J Assoc Res
791 Otolaryngol *13*, 199-208.

792 Perkins, R.E., and Morest, D.K. (1975). A study of cochlear innervation patterns in cats and rats
793 with the Golgi method and Nomarkski Optics. The Journal of comparative neurology *163*, 129-
794 158.
795 Petralia, R.S., Esteban, J.A., Wang, Y.X., Partridge, J.G., Zhao, H.M., Wenthold, R.J., and
796 Malinow, R. (1999). Selective acquisition of AMPA receptors over postnatal development
797 suggests a molecular basis for silent synapses. Nature neuroscience *2*, 31-36.
798 Pujol, R., and Carlier, E. (1982). Cochlear synaptogenesis after sectioning the efferent bundle.
799 Brain research *255*, 151-154.
800 Pujol, R., Carlier, E., and Devigne, C. (1978). Different patterns of cochlear innervation during
801 the development of the kitten. J Comp Neurol *177*, 529-536.
802 Pujol, R., Lenoir, M., Robertson, D., Eybalin, M., and Johnstone, B.M. (1985). Kainic acid
803 selectively alters auditory dendrites connected with cochlear inner hair cells. Hearing research *18*,
804 145-151.
805 Roux, I., Wersinger, E., McIntosh, J.M., Fuchs, P.A., and Glowatzki, E. (2011). Onset of
806 cholinergic efferent synaptic function in sensory hair cells of the rat cochlea. J Neurosci *31*,
807 15092-15101.
808 Ruel, J., Bobbin, R.P., Vidal, D., Pujol, R., and Puel, J.L. (2000). The selective AMPA receptor
809 antagonist GYKI 53784 blocks action potential generation and excitotoxicity in the guinea pig
810 cochlea. Neuropharmacology *39*, 1959-1973.
811 Ruel, J., Wang, J., Rebillard, G., Eybalin, M., Lloyd, R., Pujol, R., and Puel, J.L. (2007).
812 Physiology, pharmacology and plasticity at the inner hair cell synaptic complex. Hear Res *227*,
813 19-27.

814 Ruggero, M.A., Santi, P.A., and Rich, N.C. (1982). Type II cochlear ganglion cells in the
815 chinchilla. Hear Res *8*, 339-356.
816 Ryan, A.F., Woolf, N.K., and Bone, R.C. (1980). Ultrastructural correlates of selective outer hair
817 cell destruction following kanamycin intoxication in the chinchilla. Hearing research *3*, 335-351.
818 Safieddine, S., and Eybalin, M. (1995). Expression of mGluR1 alpha mRNA receptor in rat and
819 guinea pig cochlear neurons. Neuroreport *7*, 193-196.
820 Schmitz, F., Konigstorfer, A., and Sudhof, T.C. (2000). RIBEYE, a component of synaptic
821 ribbons: a protein's journey through evolution provides insight into synaptic ribbon function.
822 Neuron *28*, 857-872.
823 Sheng, M. (1997). Excitatory synapses. Glutamate receptors put in their place. Nature *386*, 221,
824 223.
825 Sheng, M., and Kim, E. (2000). The Shank family of scaffold proteins. Journal of cell science
826 *113 (Pt 11)*, 1851-1856.
827 Simmons, D.D., and Liberman, M.C. (1988a). Afferent innervation of outer hair cells in adult
828 cats: I. Light microscopic analysis of fibers labeled with horseradish peroxidase. The Journal of
829 comparative neurology *270*, 132-144.
830 Simmons, D.D., and Liberman, M.C. (1988b). Afferent innervation of outer hair cells in adult
831 cats: II. Electron microscopic analysis of fibers labeled with horseradish peroxidase. The Journal
832 of comparative neurology *270*, 145-154.
833 Sobkowicz, H.M., Slapnick, S.M., and August, B.K. (1993). Presynaptic fibres of spiral neurons
834 and reciprocal synapses in the organ of Corti in culture. Journal of neurocytology *22*, 979-993.
835 Spoendlin, H. (1971). Primary structural changes in the organ of Corti after acoustic
836 overstimulation. Acta oto-laryngologica *71*, 166-176.

837 Spoendlin, H. (1975). Neuroanatomical basis of cochlear coding mechanisms. Audiology *14*,
838 383-407.
839 Thiers, F.A., Nadol, J.B., Jr., and Liberman, M.C. (2008). Reciprocal synapses between outer
840 hair cells and their afferent terminals: evidence for a local neural network in the mammalian
841 cochlea. J Assoc Res Otolaryngol *9*, 477-489.
842 Toth, K., and McBain, C.J. (1998). Afferent-specific innervation of two distinct AMPA receptor
843 subtypes on single hippocampal interneurons. Nature neuroscience *1*, 572-578.
844 Tsubokawa, H., Oguro, K., Masuzawa, T., Nakaima, T., and Kawai, N. (1995). Effects of a
845 spider toxin and its analogue on glutamate-activated currents in the hippocampal CA1 neuron
846 after ischemia. Journal of neurophysiology *74*, 218-225.
847 Usami, S., Matsubara, A., Fujita, S., Shinkawa, H., and Hayashi, M. (1995). NMDA (NMDAR1)
848 and AMPA-type (GluR2/3) receptor subunits are expressed in the inner ear. Neuroreport *6*,
849 1161-1164.
850 Wagner, H.J. (1997). Presynaptic bodies ("ribbons"): from ultrastructural observations to
851 molecular perspectives. Cell Tissue Res *287*, 435-446.
852 Wang, Q., and Green, S.H. (2011). Functional role of neurotrophin-3 in synapse regeneration by
853 spiral ganglion neurons on inner hair cells after excitotoxic trauma in vitro. J Neurosci *31*, 7938-
854 7949.
855 Weisz, C., Glowatzki, E., and Fuchs, P. (2009). The postsynaptic function of type II cochlear
856 afferents. Nature *461*, 1126-1129.
857 Weisz, C.J., Lehar, M., Hiel, H., Glowatzki, E., and Fuchs, P.A. (2012). Synaptic transfer from
858 outer hair cells to type II afferent fibers in the rat cochlea. The Journal of neuroscience : the
859 official journal of the Society for Neuroscience *32*, 9528-9536.

860 Zachary, S.P., and Fuchs, P.A. (2015). Re-Emergent Inhibition of Cochlear Inner Hair Cells in a
861 Mouse Model of Hearing Loss. J Neurosci *35*, 9701-9706.
862 Zenisek, D., Davila, V., Wan, L., and Almers, W. (2003). Imaging calcium entry sites and ribbon
863 structures in two presynaptic cells. J Neurosci *23*, 2538-2548.
864
865
866
867
868
869 **FIGURE LEGENDS**
870
871 **Figure 1**. Ribbons and AMPAR clusters in cochlear whole mounts. Maximum intensity
872 projections of confocal z-stacks of the medial region of the organ of Corti from an adult rat
873 viewed from the endolymphatic surface including 24 adjacent OHCs and 5 IHCs. A. OHCs:
874 immunolabel for the presynaptic ribbon marker (CtBP2: red channel). Immunolabel for the
875 postsynaptic marker glutamate receptor A2 (GluA2: green channel). Merged and magnified
876 inserts: CtBP2 and GluA2 puncta overlapped in the X-Y plane. Rotation to the Z-X or Z-Y planes
877 reveals displacement between pre- and postsynaptic markers. B. IHCs: pre- and postsynaptic
878 immunolabels. CtBP2 (red) and GluA2 (green) immunopuncta were consistently juxtaposed at
879 the IHCs. Magnified insert in the X-Y plane shows clear separation of pre- and postsynaptic
880 labels. X-Z and Z-Y labels not as well-segregated as in OHCs. C. Quantification of the number
881 and the percentage of juxtaposed CTBP2 and GluA2 puncta in OHCs. D. Quantification of the

882 number and the percentage of juxtaposed CtBP2 and GluA2 puncta in the IHCs. n=3-9
883 independent preparations; 50 IHCs, 72 OHCs for panels A-D. There were no statistically
884 significant differences in number or correlation among the immunolabels (one way-ANOVA test;
885 p>0.05). Scale bar is 5 for A and B panels, and 2.5 µm in magnified inserts.
886
887 **Figure 2**. AMPA receptors mediate synaptic transmission from OHC to type II afferents in young
888 (1-2 week old) rat cochlea. A. Inward synaptic currents (small downward deflections) evoked by
889 high potassium saline were reduced, then eliminated by exposure to CP-465,022. B. Diary plot
890 showing partial block of EPSCs by 1 µM CP465,022 followed by complete block by 10 µM, then
891 partial recovery after washout. Recordings (Vhold -80 mV) were made in 40mM external
892 potassium to increase EPSC frequency. C. Cumulative fraction plot of EPSCs from fiber in B.
893 EPSC amplitudes decreased in the presence of 1µM CP465,022 (red). D. Scaled EPSC waveforms
894 before (black) and during exposure to 1µM CP465,022 (red) showing identical kinetics.
895
896 **Figure 3.** Calcium-impermeant glutamate receptors carry synaptic currents in type II afferents
897 in young (1-2 week old) rat cochlea. A. Averaged synaptic currents in type II fiber containing
898 100 µM spermine at indicated membrane potentials (not corrected for junction
899 potential). Numbers of events in each average range from 115 to 624. B. Current-voltage curve
900 of synaptic currents for spermine-loaded type II fiber (red) compared to control data (black from
901 Weisz et al., 2009, used with permission). Average current amplitude with standard deviations
902 shown for spermine data. C. Average synaptic currents in a type II fiber (average over 10
903 second bins) before (black) and during exposure to 20 µM philanthotoxin (mean with standard

deviation). D. Average synaptic currents in a type II fiber (average over 10 second bins) before (black) and during exposure to 10 μM Naspm (mean with standard deviation).

Figure 4. IHC synaptic immunopuncta. Confocal z-stacks of 5 IHCs in the middle turn of the organ of Corti from an adult rat viewed from the endolymphatic surface. A, B. Immunolabeling for postsynaptic density proteins; PSD95 (red channel) and Shank (green channel) (A) or Homer (green channel) (B) show closely coincident puncta of these postsynaptic density markers (magnified inserts in the X-Y plane). C. Immunolabeling for CtBP2- red channel, and the postsynaptic marker PSD95. Magnified insert shows juxtaposition in the X-Y plane. D. Immunolabel comparing CtBP2 and Shank distribution. E. Immunolabel comparing CtBP2 and Homer. F. Quantification of pre- and postsynaptic immunopuncta in IHCs. G. Quantification of percentage juxtaposition of postsynaptic density proteins. H. Quantification of percentage juxtaposition for presynaptic ribbon marker CtBP2 and the postsynaptic density proteins (PSD95, Shank and Homer). A-H: n= 40-60 IHCs from 4-5 independent preparations. There were no statistically significant differences in number or correlation among these immunopuncta (one way-ANOVA test; $p>0.05$). Scale bar is 5 μm or 2.5 μm for low and high magnifications, respectively.

Figure 5. OHC synaptic immunopuncta. Confocal z-stack of OHCs in the middle turn of the organ of Corti from an adult rat viewed from the endolymphatic surface. A. Immunolabeling with the postsynaptic density proteins PSD95 (red channel) and Shank (green channel) show an

interconnected series of puncta along the base of the OHCs. PSD95 and Shank puncta are closely coincident (magnified insert, X-Y plane). B. Immunolabeling with the presynaptic ribbon marker CtBP2 (red) and postsynaptic marker Shank (green). C. Immunolabel for CtBP2 (red) and PSD95 (green). D. Immunolabel for CtPB2 (red) and Homer (green). Magnified inserts (X-Y plane) in each case show more extensive postsynaptic density distribution than presynaptic ribbon label. E. Pre- and postsynaptic immunopuncta at the OHCs. There were significantly fewer CtBP2 or GluA2 puncta than postsynaptic density puncta (PSD95, Shank or Homer) (one way-ANOVA, $p = 0.01$; Bonferroni's multiple comparison test; $n = 3$-7; 72-168 OHCs). F. Thumbnails of the base of individual OHCs immunolabeled for CtBP2 (red channel) and Shank (green channel). Many Shank immunopuncta had no associated CtBP2 puncta. G. Thumbnails of the base of individual OHCs immunolabeled for GluA2 (red channel) and Shank (green channel). Many of the Shank immunopuncta had no associated GluA2 puncta. H. Percent Juxtaposition of the CtBP2 and postsynaptic density proteins (PSDs). The ratio of PSD95, Shank or Homer puncta juxtaposed to CTBP2 was significantly smaller than the ratio of CTBP2 puncta juxtaposed to the postsynaptic density proteins (one way-ANOVA test; $p \leq 0.01$; Bonferroni's multiple comparison test); i.e., many PSDs had no ribbon. Scale bar is 5 µm in wide-view and 2.5 µm in magnified inserts and thumbnails. I. Schematic drawing of OHC and IHC synapses. At the IHC afferent synapse CtBP2/GluA2 relates closely in number to postsynaptic density markers. At the OHC afferent synapse, only a subset of postsynaptic density proteins relates to CtBP2/GluA2 synaptic markers.

947 **Figure 6**. Single type II fibers visualized by intracellular labeling. A. Apical turn of a young (P8)
948 rat organ of Corti with biocytin filled type II fiber after streptavidin-peroxidase reaction. Scale
949 bar 125 µm. B. Higher magnification of boxed areas in A – showing trajectory and terminal
950 branches. C. Biocytin-filled type II fiber reacted with streptavidin-AlexaFluor488 (green). OHC
951 nuclei labeled with DAPI (blue). Magnifications show en passant (red arrows) and terminals
952 (white arrowheads) swellings of branches from boxed regions. D. Biocytin-streptavidin-
953 AlexaFluor488 filled fiber combined with FM1-43-labelled OHCs (red). Magnifications show
954 terminal branches enwrapping the base of outer hair cells. E. Biocytin-streptavidin-
955 AlexaFluor488 filled fiber combined with CtPB2 immunolabel (red). Magnifications show
956 approximation of some terminal branches to CtBP2 puncta. F. Combined immunolabel for
957 PSD95 (green) and CtBP2 (red) among OHCs of young rat cochlea. Magnification shows 'pearl
958 chain' pattern found in adult cochlea. Scale bar 5µm in B, C, D, E, F, G; 2.5µm in all
959 magnifications.
960
961 **Table 1.** Morphology of biocytin-filled type II fibers in the apical turn of young rat cochleas. 15
962 individually labeled fibers (intracellular recording with biocytin-containing pipette) were
963 measured. Distance to apex in column 3 is from the point of crossing the tunnel of Corti.
964 'Distance to apex' in the major synaptic area is from the centerpoint of the region of terminal
965 branches.
966

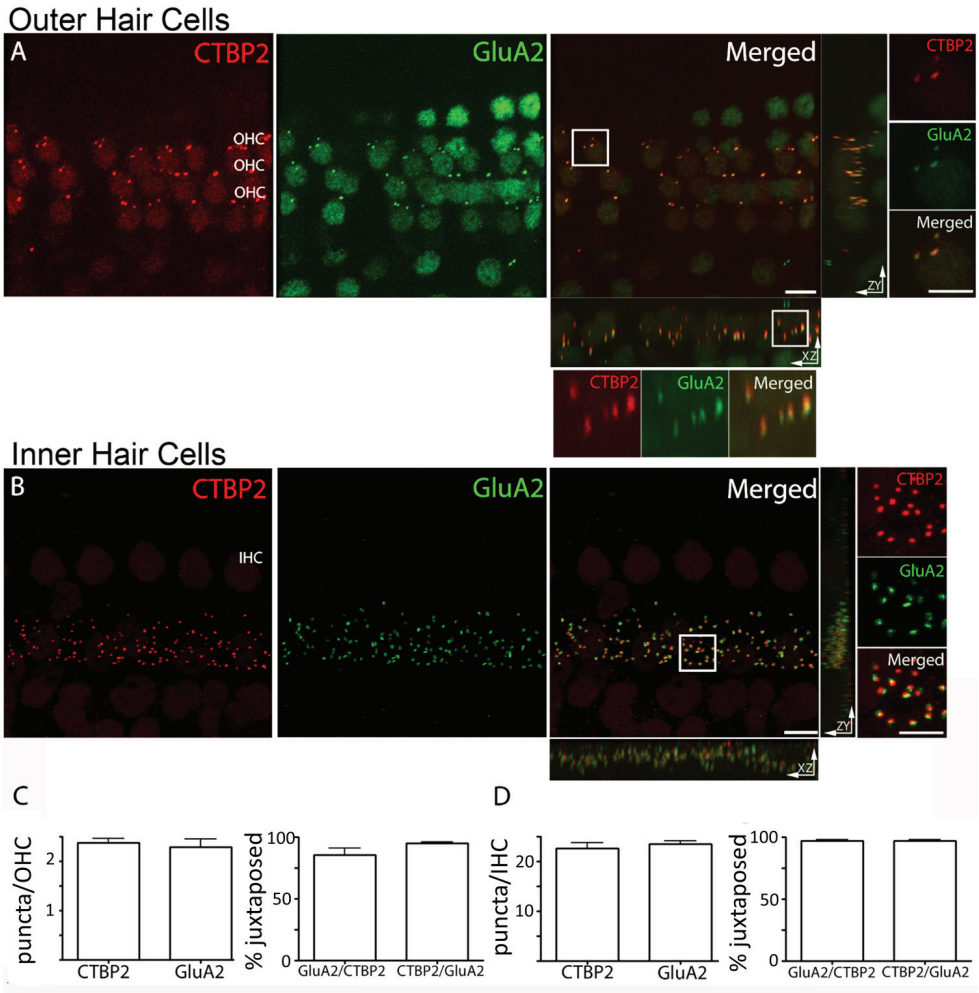

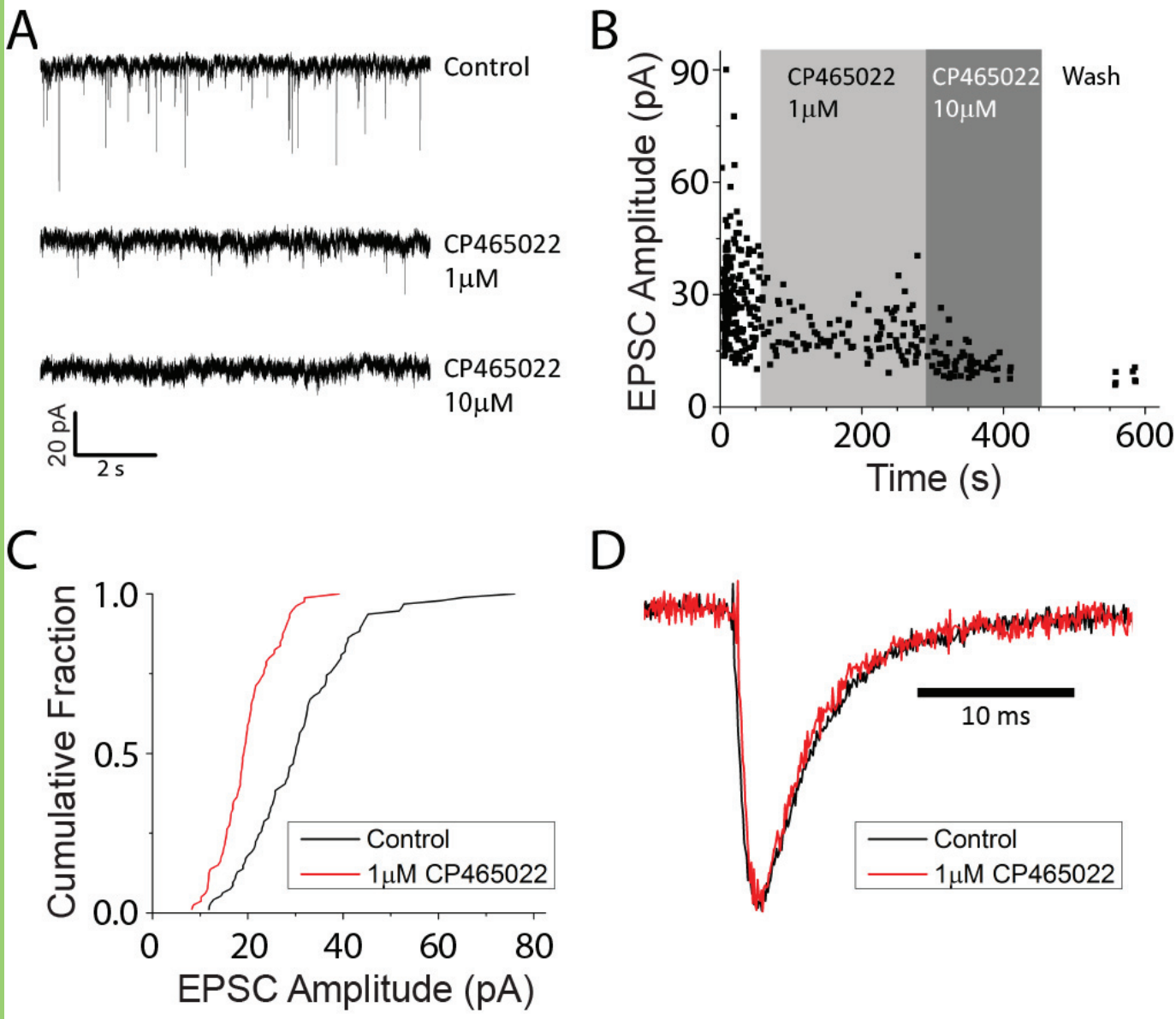

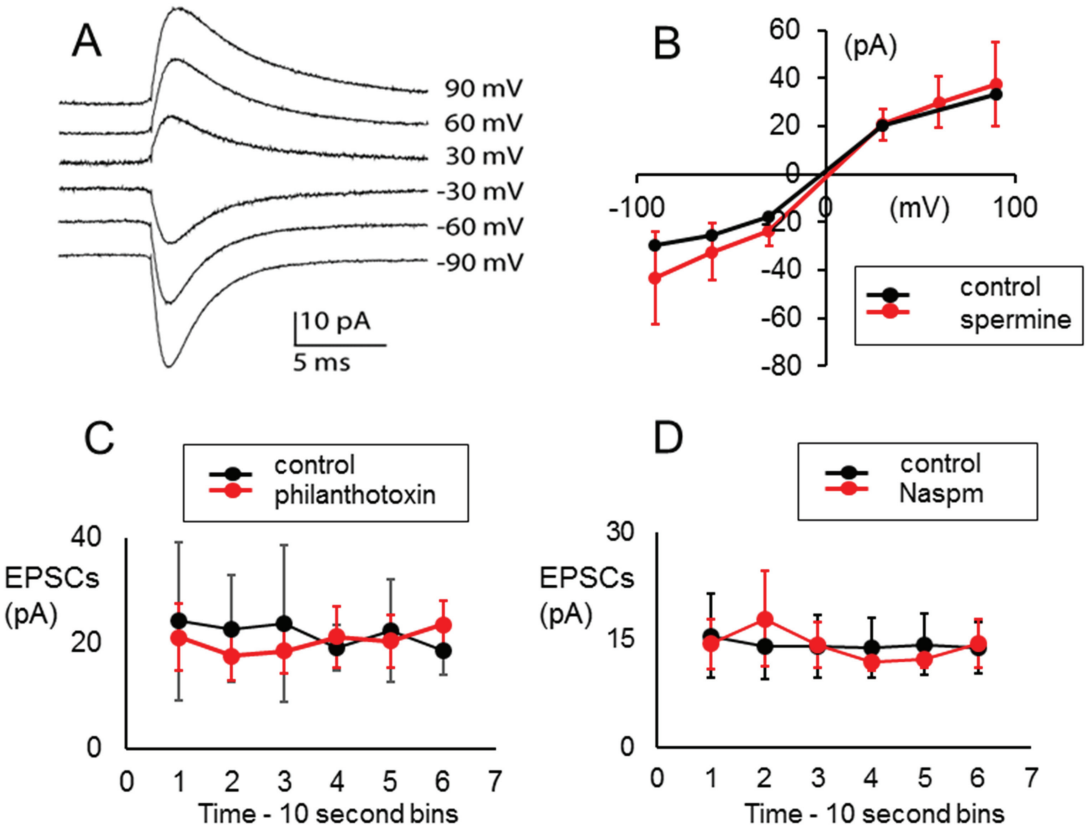

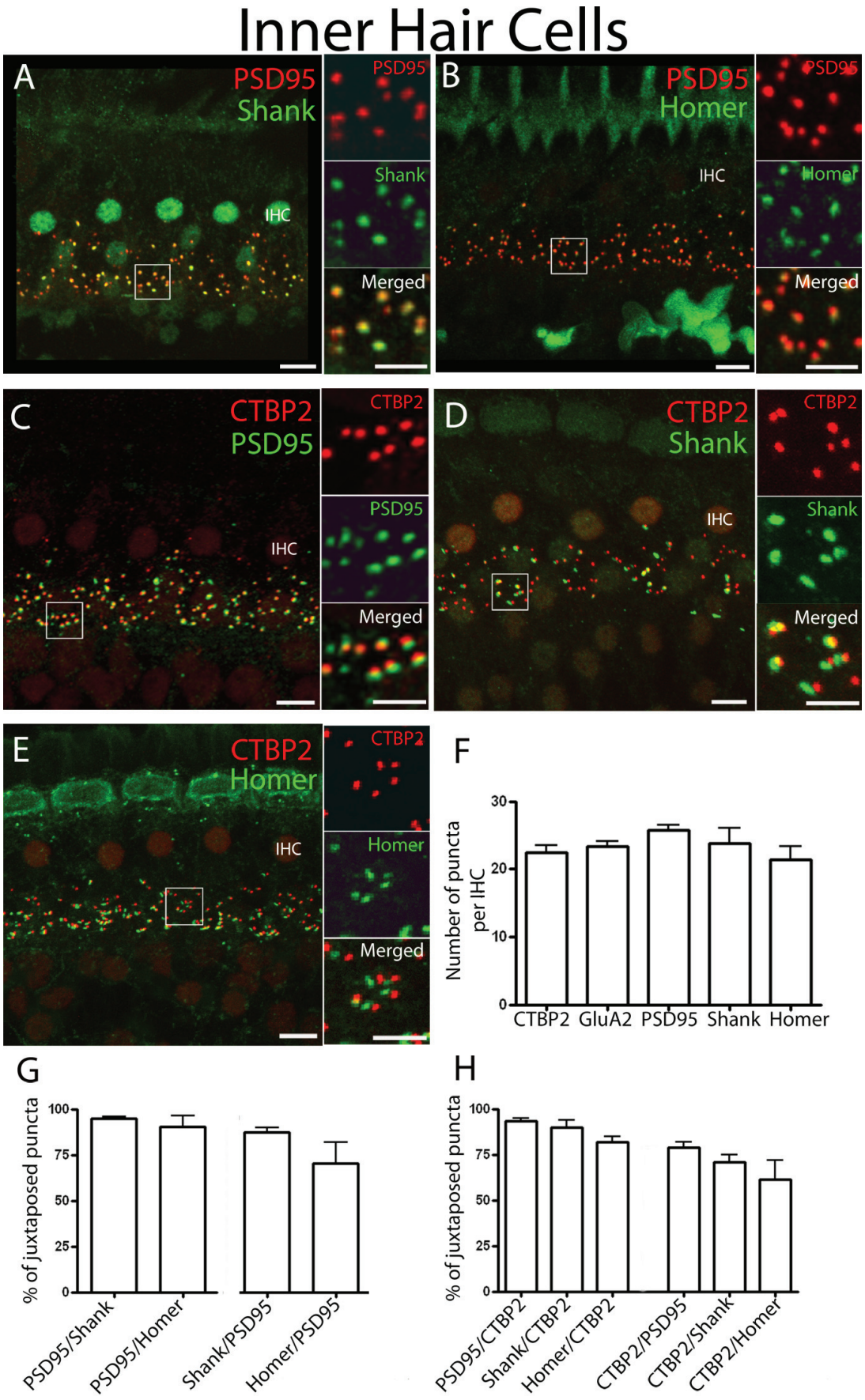

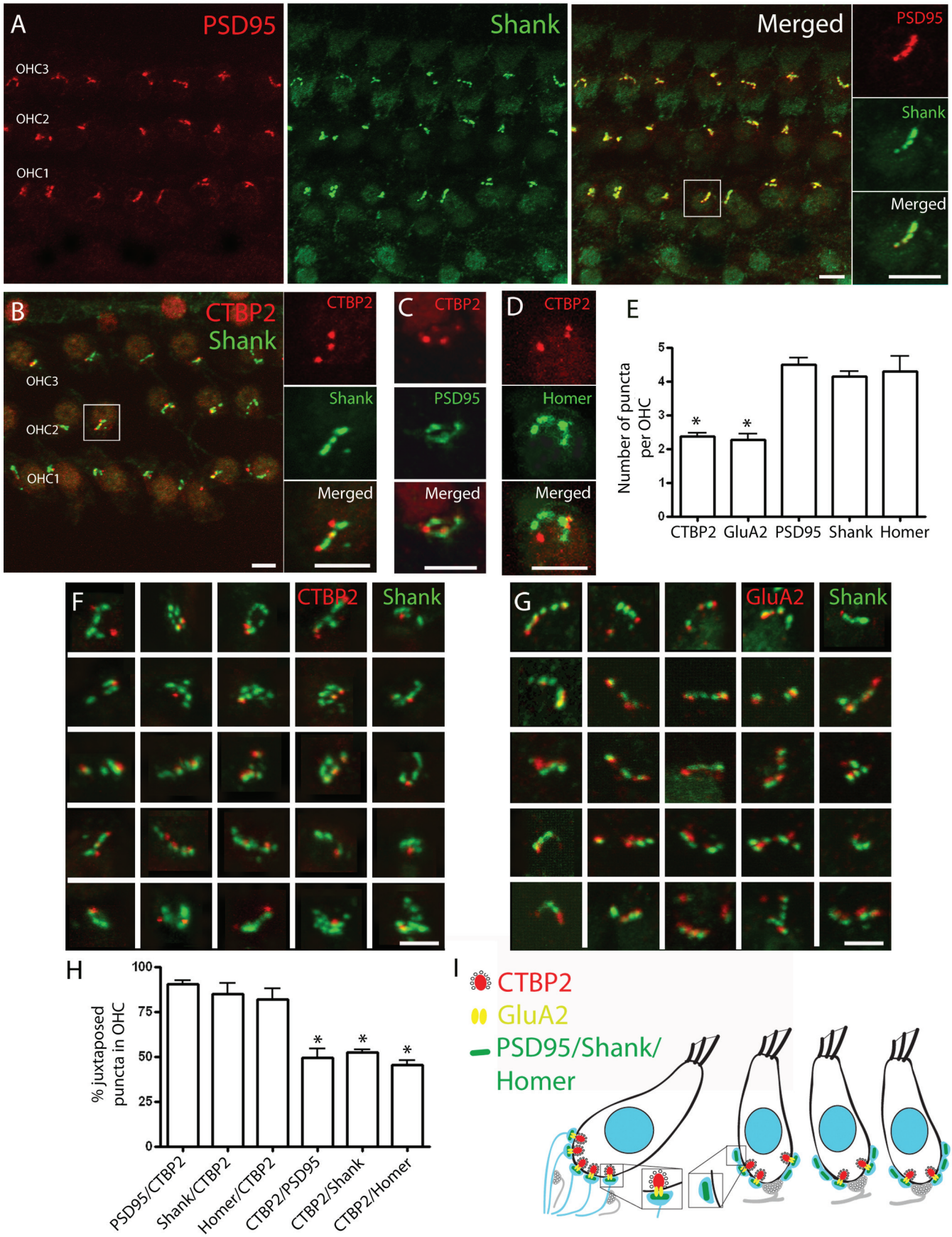

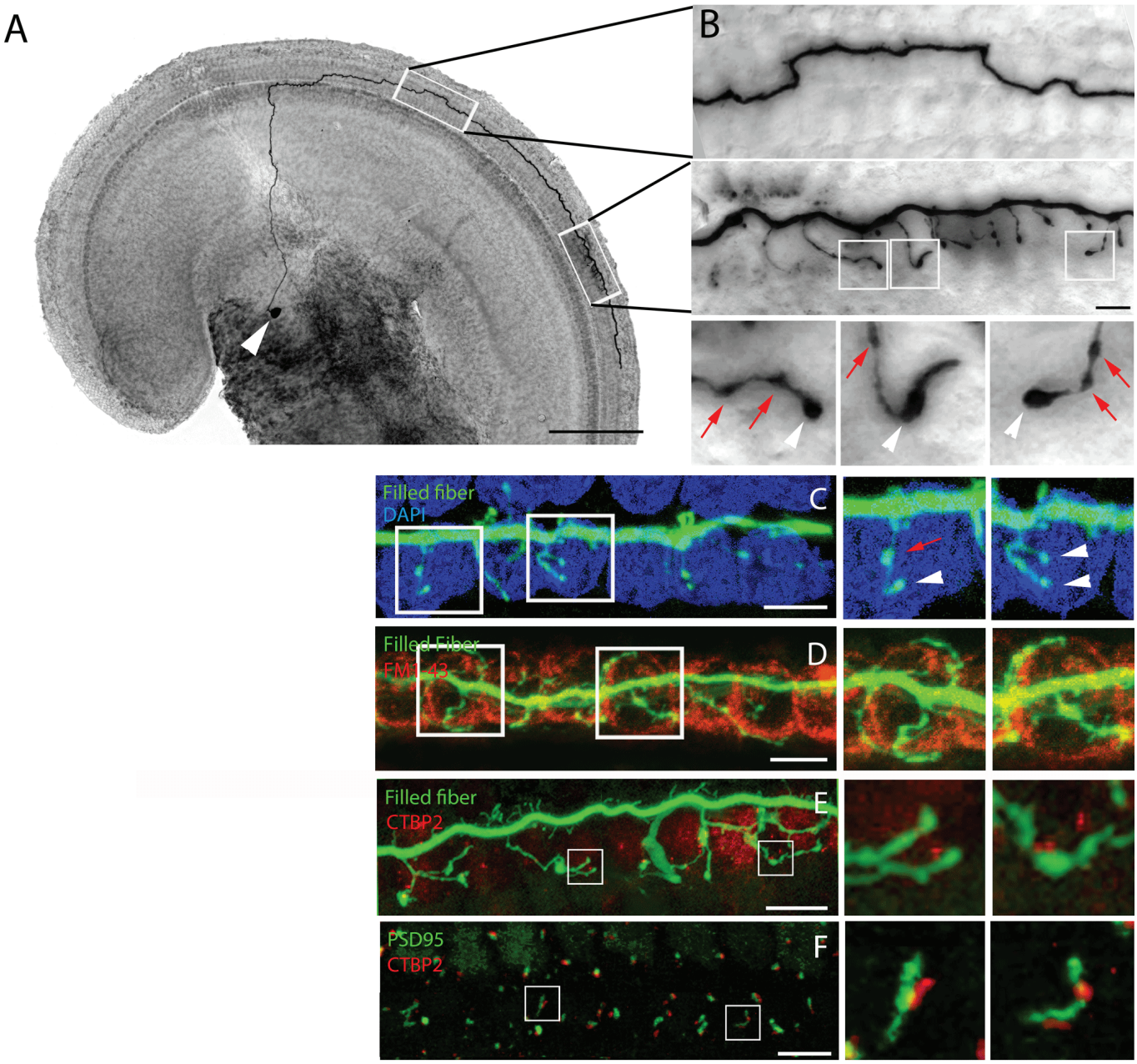

Table 1: Morphology of biocytin-filled type II fibers in the apical turn of young rat cochleas							
Fiber number	Spiral process (µm)	Distance to apex (µm)	Number of arbors	Total synaptic branches	Major synaptic area		
					Distance from apex	Length	No. of branches
1	899.2	843	1	21	1532	97.3	13
2	516.4	1121	1	13	1448.3	150.2	9
3	1194.7	566.5	1	21	1618.3	165.2	11
4	617.8	613.5	1	12	1082.2	160.5	12
5	585.5	997.8	1	15	1109	52.8	9
6	733.9	658.1	1	22	1108.3	161.3	12
7	549.1	608	1	17	920.3	224.8	17
8	612.8	NA damage	1	13	NA	101.3	12
Average ± SEM	714±81	773±77		17±1.4	1260±95	139±19	12±1
9	400.65	488.8	2	8	692	60.9	8
10	720.1	983	2	14	1243.4	168	11
11	983	577	2	7	1255.2	139.6	7
12	689.1	613	2	20	1095.4	135.2	15
13	413.5	479.5	3	24	700	130.245	18
14	475.5	919	2	13	1107.8	149.5	13
15	649.7	924	2	23	1423.4	193.4	20
Average ± SEM	619±79	712±83		16±3	1074±106	140±15	13±2
Total Average ± SEM	669±56	742±55		16±1	1167±72	139±12	12±1

Table 1. Morphology of biocytin-filled type II fibers in the apical turn of young rat cochleas. 15 individually labeled fibers (intracellular recording with biocytin pipette) were measured. Distance to apex in column is from the point of crossing the tunnel of Corti. 'Distance to apex' is from the centerpoint of the region of terminal branches in the major synaptic area.